Universiteit Utrecht

Zeolitic Imidazolate Frameworks

Thin Film Syntheses
Post-Synthetic Cation Exchange in Bulk Material and its Catalytic Applications

Thesis for the degree of Master of Science

In the Graduate School of Natural Sciences

Debye Institute for Nanomaterials Science

Inorganic Chemistry and Catalysis

By Thomas Hartman, BSc.

Supervised by:
Zafer Öztürk, MSc.
Rogier Brand, MSc.
Dr. Pieter C.A. Bruijnincx
Prof. Dr. Ir. Bert M. Weckhuysen

Abstract

In this thesis, multiple approaches for the use of Zeolitic Imidazolate Frameworks (ZIFs) are reported and described in three chapters:

Chapter 1 – Surface Mounted Imidazolate Frameworks
An attempt was made to gain control over the growth of ZIFs on gold surfaces functionalized with specific thiols. With the use of carboxylic acid-, imidazole- and methyl-terminated SAMs, no homogeneous growth was observed. This result was ascribed to a bad quality of gold coated silicon wafers. Characterization of the products was performed with AFM, grazing Angle IR and contact angle measurements.

Chapter 2 – Post-synthetic Cation Exchange (PScE)
A method to exchange zinc ions in the framework with manganese ions from solution was reproduced from Fei *et al.*[1] With atomic absorption spectrometry (AAS), inductively coupled plasma optical emission spectrometry (ICP-OES), X-ray photoelectron spectroscopy (XPS) and energy dispersive X-ray spectroscopy (EDX), exchange yields were observed to be 2-20% after an exchange period of 1 day; this was increased to a maximum of 35% after 3 days. Although it was proven that the particles did not leach zinc or manganese ions, no evidence was found with X-ray diffraction (XRD), XPS and N_2-physisorption that manganese was truly incorporated into the framework.

Chapter 3 – Catalytic Testing of ZIF-8 [$Zn_{1-x}Mn_x$]
Exchanged ZIF-8 crystals were used as a catalyst in the oxidation reaction of veratryl alcohol to veratraldehyde and in the epoxidation of olefins. An increase in the conversion of veratryl alcohol was measured with Gas Chromatography (GC). Additionally, no leaching of metal ions was observed with ICP-OES and after hot-filtration. The ZIF-8 [$Zn_{1-x}Mn_x$] material exhibited no catalytic activity in the epoxidation of olefins.

Acknowledgements

This thesis would not have been here as it is now without the help of many people, and I would like to thank them in this chapter.

First and foremost, I would like to thank the group and in particular Bert Weckhuysen for giving me the opportunity to work on this project. I would also like to thank Bert Weckhuysen for his advices and suggestions during the group discussions.

Also, I would sincerely like to thank Pieter Bruijnincx for his supervision. Not only have you helped me to get the research on the right track with many great advices, but you were also very helpful when I came into your office with questions unrelated to my research. It has always been a pleasure to have discussions with you.

Two important persons for my Master thesis were my daily supervisors Zafer and Rogier. Zafer, you once told me that you felt bad that you could not be here during the first 6 months of my research. I will say it once more: it was not your fault! You did everything you could and what is more important, you were here the second half and did everything you could to help me obtaining a great result. Thank you for all of this! It has been a very pleasant time working with you and I hope that you will stay healthy for a very long time! I hope to stay in contact with you, and I will surely let you know about my time in Warwick (and after). Rogier, despite of the fact that you had a very busy period with supervising me and Jochem on your own the first months; you were still there for me and helped me in the way only you can. With an unprecedented patience and calmness you were able to teach me all the things I needed to know, and more. Many thanks for all the help you have given me and for the pleasant working experience!

Furthermore, I would like to thank all of the following persons who have helped me with the characterization techniques used in this thesis: Jan Philipp Hofmann and Quanbao Ma (XPS), Adelheid Elemans-Mehring (ICP-OES), Joe Stewart (TGA), Marjan Versluijs-Helder (XRD, SEM and EDX), Arjan den Otter (N_2-physisorption) and Fouad Soulimani (IR spectroscopy). Jan Philipp, I would also like to thank you for the discussions we had and the advice you gave me!

Finally I would like to thank the people that indirectly have made my stay here more amusing. My fellow Master students at the balcony: Karst, Tanja, Tom and Wouter. Thank you for all the nice/funny/interesting/weird discussions we had and videos we have watched!

Contents

Abstract 3
Acknowledgements 4
List of Abbreviations 7
Introduction 9
Chapter 1 11
1.1 Introduction 12
1.2 Theory 14
1.2.1 Solvothermal synthesis of MOFs 14
1.2.2 Syntheses strategies for thin films of metal organic frameworks 14
1.2.3 Aqueous room temperature syntheses 17
1.2.4 Self-assembled monolayers 18
1.3 Methods 21
1.3.1 Materials 21
1.3.2 Bulk syntheses 21
1.3.3 SAMs preparation 22
1.3.4 Thin film syntheses 22
1.4 Results and discussion 24
1.4.1 Layer-by-layer synthesis 24
1.4.2 Self-Assembled Monolayers 26
1.4.3 Quality of gold coated substrates 28
1.5 Conclusions 30
1.6 Outlook 30
Chapter 2 31
2.1 Introduction 32
2.2 Theory 35
2.2.1 Post-synthetic Cation Exchange 35
2.2.2 Stabilities and preferred geometries 36
2.3 Methods 38
2.3.1 Materials 38
2.3.2 ZIF-8 synthesis in methanol 38
2.3.3 Post-synthetic cation exchange 38
2.4 Results and Discussion 39
2.4.1 Metal concentration 39
2.4.2 Towards higher reproducibility 41
2.4.3 Increase in metal concentration after exchange 42

2.4.4 Framework disruption 43
2.5 Conclusions 47
2.6 Outlook 47
2.6.1 Alter the exchange conditions 47
2.6.2 Exchange with other metals 48
2.6.3 Characterization Techniques 48
Chapter 3 49
3.1 Theory ..... **Error! Bookmark not defined.**
3.2 Methods 52
3.2.1 Materials 52
3.2.2 Oxidation of Veratryl Alcohol 52
3.2.3 Peroxidation of Olefins 52
3.3 Results and discussion 53
3.3.1 Epoxidation of olefins 53
3.3.2 Oxidation of veratryl alcohol 53
3.3.3 The catalyst 54
3.4 Conclusions 56
3.5 Outlook 56
Chapter 4 57
4.1 Infrared and Raman Spectroscopy 58
4.2 Gas Chromatography 60
4.3 X-Ray Diffraction 61
4.4 Contact Angle Measurements 61
4.5 Thermogravimetric Analysis 62
4.6 N_2 Physisorption 63
4.7 Atomic Absorption Spectrometry 64
4.8 Inductively Coupled Plasma Optical Emission Spectrometry 66
4.9 X-ray Photoelectron Spectroscopy 67
4.10 Scanning Electron Microscopy and Energy Dispersive X-ray Spectroscopy 68
4.11 Atomic Force Microscopy 69
References 71
Appendix ..... **Error! Bookmark not defined.**

List of Abbreviations

AAS	Atomic Absorption Spectroscopy
AFM	Atomic Force Microscopy
DMF	Dimethylformamide
EDC	1-ethyl-3-(3-dimethylaminopropyl)-carbodiimide
EDX	Energy Dispersive X-Ray Spectroscopy
FTIR	Fourier Transform Infrared
GC	Gas Chromatography
HmIm	2-methylimidazole
ICP-OES	Inductively Coupled Plasma Optical Emission Spectroscopy
LbL	Layer-by-layer
LPE	Liquid Phase Epitaxy
MHDA	16-Mercaptohexadecanoic acid
MOF	Metal Organic Framework
NHS	N-hydroysuccinimide
ODT	Octadecanethiol
PScE	Post-synthetic Cation Exchange
PSE	Post-synthetic Exchange
SAM	Self-Assembled Monolayer
SEM	Scanning Electron Microscopy
SURMOF	Surface Mounted Metal Organic Framework
SURZIF	Surface Mounted Zeolitic Imidazolate Framework
TEA	Triethylamine
TGA	Thermogravimetric Analysis
XPS	X-Ray Photoelectron Spectroscopy
XRD	X-Ray Diffraction
ZIF	Zeolitic Imidazolate Framework
ZIF-8 [$Zn_{1-x}Mn_x$]	ZIF-8 of which a fraction of zinc (x) is exchanged with manganese

Introduction

In modern society, porous materials are of great value for enhancing the quality of the products we use and consume and therefore have a large impact on our lifestyles. An example of a class of porous materials with historical importance is the class of zeolites. Due to their porous structure, these materials exhibit a very high surface area in comparison to normal, bulk materials. They do not only have interaction with matter at the outer surface, but can also interact throughout the bulk of the material as a result of their porous structure. [2]

Since the introduction of the zeolites faujasite X and Y in the early 1960s and not much later ZSM-5, their high surface area in combination with their acid surfaces and high stability have been used to improve the efficiency of the cracking of oil in the petrochemical industry.[3] Since then, researchers all over the world have not been standing still, and are still working on improving efficiencies.[4] In the everyday life we are using zeolites as water softeners in washing powders. They are able to adsorb calcium ions from the solution and replace them with sodium ions, which were previously bound to the surface. This ion-exchange method can also be adopted to purify water sources.[5]

A newer and more unknown class of porous materials consists of Coordination Polymers. These materials are built up from metal ions or metal clusters which are bridged by organic ligands, usually terminated by carboxylic acids. When porous structures are made, the products are called a porous coordination polymer (PCP), of which the first one was published in 1989 already.[6] In this article the authors discuss the many possible applications of MOFs, but it was not until 1995 that the term Metal Organic Framework (MOF) was invented.[6]

For MOFs, almost any metal can be chosen as node and there are even more options in choosing organic linkers, where one has the option to vary their length[7], functional group[8] or flexibility[9]. These properties can be used to create a very versatile material and therefore it has gotten increased attention over the last fifteen years and attention is still increasing steeply (Figure 1).[10]

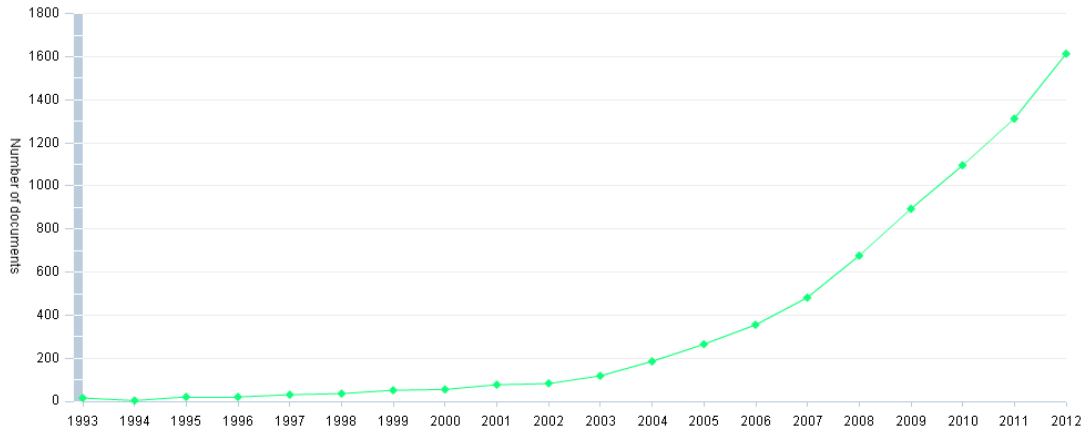

Figure 1. A steep incline can be seen in the number of articles reporting on MOFs from the year 2002 and beyond (search performed by Scopus with the following keywords: Metal Organic Framework).

Not only the great variety in all the different topologies of MOFs causes the large interest in this material, but MOFs also exhibit some unique properties which have not been seen in other porous materials. The surface area can be extremely large; some MOFs have shown a Brunauer-Emmett-

Teller (BET) surface area of larger than 7000 m^2g^{-1} [11] and with different ligands, the functionality of the MOFs can be altered, even within one phase.[8]

Owing to high versatility of MOFs and the possibility to fabricate numerous different structures, a new subclass of MOFs arose which has a similar structure to zeolites. Zeolitic Imidazolate Frameworks (ZIFs) are built up from metal nodes, bridged by imidazolates through the nitrogen atoms in the 1,3-position. The bridging angles between imidazoles and two metal nodes are close to 145° (Figure 2); this is exactly the same angle that can be found between two silicon atoms linked by oxygen in zeolites. There is room to choose from all derivatives of imidazole, or even a combination of derivatives which means that a very versatile material can be prepared like with MOFs, although the choice of metal is mainly cobalt or zinc.[12] Other variations can be transition metals that can be incorporated within the pores.[13] Due to their similar structure to zeolites and the many possibilities in starting materials, ZIFs combine the higher chemical and thermal stability of zeolites with the chemical diversity of MOFs and could play a crucial role in the development of new catalysts.

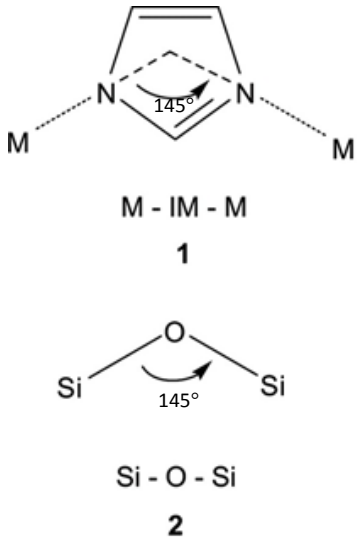

Figure 2. Both angles of Si-O-Si and M-IM-M are 145°.[9]

This thesis will focus on ZIFs and consists of three chapters that contain information on two different applications for this material. The first chapter is about the attempt to grow thin films of ZIF-8 on a substrate with the liquid phase epitaxy method. The second chapter is about exchanging the zinc ions from the framework with manganese ions in solution. The goal is to reproduce the experiments by Fei *et al*. and to optimize this method. In addition, the new types of ZIF-8 were used as a catalyst in epoxidation reactions of olefins and the oxidation of veratryl alcohol to veratraldehyde. The results of these reactions are discussed in the third chapter.

The methods and theory of the instruments that were used for the characterization of the products can be found in the fourth chapter.

Chapter 1

SURFACE MOUNTED IMIDAZOLATE FRAMEWORKS

1.1 Introduction

Surfaces are of great importance, it is not only just the outermost boundary of a material; it dictates how materials interact with their environment at the interface. This is the reason why scientists from many different fields such as the energy or medical industry are interested in the surfaces of the materials they are using; do they have the right properties to be used in the environment they work in or how could we alter their surfaces to our best benefit?[14]

Coating materials has long been a topic of interest to people; in fact, millennia ago the Egyptians already used coating techniques to preserve their statues. To date, different techniques and coatings have been used to alter the surface of materials with respect to durability, strength and appearance. In modern science, biochemists tailor the surfaces of toxic materials so that they become biocompatible materials, whereas scientists from the energy industry are focused on making catalysts more robust and efficient by altering the surfaces.[15]

The potential of tailoring the surface of materials becomes more and more apparent, with the ultimate goal of creating a material with a surface that is customizable from a distance by remote control. For this purpose, porous materials could prove of significant value. By coating a material with a thin film of a porous material, it is possible to change the properties of the surface by loading the pores of the porous surface with different functional molecules or particles. Depending on the porous material and on the molecules or particles, this can be reversible or not. Another interesting property that porous materials could provide, is the function of a molecular sieve at the surface. In terms of catalysis, this approach could lead to a higher size-selectivity; reactants smaller than the pore aperture can enter the pores, in contrast to larger molecules that cannot.

The most well-known organic porous material is activated carbon, which has surface areas of above 2000 m^2/g. However, their pores are not ordered and the shapes can vary largely. Another well-known class of porous materials is that of zeolites, mainly composed of silicon, aluminum and oxygen. Microporous and mesoporous zeolites are known and are used very often, varying from everyday products, such as washing powder, to the cracking of oil to more valuable products. Zeolites have a significantly higher thermal stability and robustness in comparison to activated carbon. Another advantage of zeolites is that their pores are well defined, and in a certain way, tunable. By choosing different syntheses procedures and by introducing different chalcogens and/or metals, over 170 different types of zeolite material have been synthesized.[16,17]

Even more freedom and flexibility could be gained when a metal organic framework (MOF) is used as a porous coating. As opposed to zeolites and activated carbon, MOFs offer the advantage of combining many different metals and linkers, enabling us to prepare highly specific coatings or membranes with molecular sieving effects. Molecular design will enable us to choose the desired pore aperture based on the linker length, and also the interaction it has with certain molecules. These special features have been tested for MOFs in the separation of harmful molecules from air and showed to be very effective, even exceeding the capacity of activated carbon to separate molecules in some experiments by a large amount.[18]

Until recently, research on MOFs has been mostly concentrated on the bulk synthesis and structure of these materials, but the potential for coating has been recognized and interest has been increasing. Not only are the possible applications interesting, but it can also give us more insight in the growth of MOFs.[19]

For the purpose of growing thin films of MOFs, new methods have been developed to enable us to grow MOFs mounted on surfaces (SURMOFs). Depositions of SURMOFs have been reported on oxidic supports as well as on functionalized surfaces. A typical functionalized surface to grow MOFs on, are carboxylic acid terminated self-assembled monolayers (SAMs) on gold coated substrates. Thiol functionalized organic linkers are deposited on gold coated substrates with a well-defined molecular arrangement and a high structural quality.[20] The carboxylic acids will then act as a first linker in the growth of the MOF crystals.

An interesting method to prepare SURMOFs is a stepwise or layer-by-layer method. In this approach, metals and linkers are added to the surface independently and step by step. This gives a high control over the size and shape of the SURMOFs, considering synthesis can be stopped after every step. This advance gives us a nearly ideal bottom-up approach for syntheses of thin film materials and may give an insight of the first growth steps with the use of atomic force microscopy (AFM) or Raman spectroscopy.

Owing to the fact that zeolitic imidazolate frameworks (ZIFs) are a relatively new subclass of MOFs, research on ZIFs is less evolved and not much research has been done on surface mounted ZIFs (SURZIFs).[21–28] As for MOFs, the method to grow ZIFs on different functionalized surfaces has already been proven to be effective,[27,29] however, a layer-by-layer method as published by Zacher *et al.*[19] and Wöll *et al.*[30]where the film thickness actually follows the expected increase in size has not been found yet. Layer by layer methods have been applied, of which the method described by Shekhah *et al*.[23] resulted in the thinnest and most homogeneous films. Still, this method does not result in a true layer-by-layer synthesis where the increase in film thickness is directly related to the size of the linkers.

As an alternative for –COOH or –OH terminated SAMs, imidazole terminated SAMs are very interesting as well, as they mimic the bridging imidazoles in ZIFs themselves; this could result in a higher understanding of their early stage crystallization. As the crystal structure of ZIFs is different from that of most other MOFs, an insight in their growth mechanism could provide the basis for zeolite (-like) growth.

The first chapter of this thesis will focus on the growth and characterization of -COOH and imidazole terminated SAMs, considering a well-defined starting material is necessary for a controlled growth of SURZIFs. Attempts to synthesize SURZIFs in a reproducible way by the layer-by-layer method on suitable SAMs were reported as well. Both SURZIFs and SAMs are characterized with grazing angle IR-spectroscopy, Raman-spectroscopy and AFM.

1.2 Theory

1.2.1 Solvothermal synthesis of MOFs

In principle, Metal Organic Frameworks (MOFs) or Zeolitic Imidazolate Frameworks (ZIFs) can simply be synthesized by the reaction of metal ions with a bridging ligand in a solution, and this is the method that has been carried out for bulk syntheses in most cases. The formation of amorphous solid phases and gels can be avoided by optimizing the conditions to where the metal-ligand bond is highly labile. Kinetic products which are formed first are able to rearrange to the thermodynamically favored product as a result of the reversible bond formation.[10]

The most widely used method to prepare MOFs in bulk quantities, is by the solvothermal or hydrothermal method, in which metal precursors and organic ligands are dissolved in organic solvents or water, respectively. The precursors and ligands will start to self-assemble at elevated temperatures, which range from 80 to 260 °C. Reactions are performed in a closed vessel or an autoclave under autogenous pressure.[31]

The synthesis of surMOFs is most of the times not that easily described, and depending on the desired properties of the material, synthesis procedures can vary.

1.2.2 Synthesis strategies for thin films of metal organic frameworks

Thin films of MOFs grown on a substrate could help to study the growth of the crystal in the early phase which could lead to a higher control over the arrangements of channels of porous modules for various nanoporous devices. There are multiple ways to grow MOFs on substrates; they can be grown on bare oxidic substrates (e.g alumina or silica) or on modified substrates with a functional group that serves as an anchoring point for the metal nodes.

The most direct and easy approach to coat a surface with a MOF, is by dipping a material into a suspension containing small MOF-crystals that were synthesized earlier in solvothermal conditions. After evaporation of the solvent, only the particles are left behind on the substrate. A disadvantage of this method is that deposition is neither selective nor uniform and it does not lead to rigid anchoring of MOF crystals on the substrate. To conclude, this method does not help to give insight in the growth of the crystal and it will not lead to a homogeneous membrane. [32]

A more advanced technique for growing SURMOFs is by using a substrate with a conductive film. By using microwave radiation the temperature near the surface of the substrate is highly increased, this will induce growth of MOFs only near the surface of the substrate and not in solution. The advantage of this method compared to the previously mentioned technique is that deposition of crystals can be performed in merely 30 seconds, which is incredibly fast in comparison to the hours or days it will takes in a typical solvothermal synthesis procedure. Unfortunately, there is a downside to this fast synthesis method; there is a high chance that unreacted metal species or organic linkers will adsorb

in the cavities of the growing MOF due to the necessity of a high concentration of precursors and this will complicate the deposition of uniform layers.[33]

A ZIF-7 (zinc metal-centers and benzimidazole linkers) membrane has been prepared by combining the two previously mentioned methods. First, a colloidal dispersion of seeding particles with an average size of 30 nm was synthesized. A dip-coating technique was used to cover the alumina disks with the ZIF-7 nanoseeds. Microwave assisted solvothermal synthesis was then carried out in an autoclave to perform secondary growth of the nanoseeds. This ZIF-7 membrane showed high permeability for H_2, but low for CO_2, N_2 and CH_4, indicating that a ZIF-7 membrane can be used for syngas separation, as the material is stable up to 500 ^{o}C.[34],[21]

A more suitable way to give rigid anchoring of crystallites is by using a functionalized surface. The nucleation and even the orientation and structure can be directed when a functional group is present on the surface of the substrate. A well-known procedure to functionalize a substrate with organic surfactants is with self-assembled monolayers (SAMs). SAMs can be synthesized rather easily by immersing gold coated substrates in a solution of organothiols. Densely packed and highly ordered and orientated monolayers will form spontaneously on the surface within a few hours. The type of organothiol, and the preparation conditions to some extent, will determine the packing density and type of defects. The quality of the SAMs is only limited to that of the substrate. Organothiols can be functionalized at the ω-position with a COOH-group so the metals can bind to the surfactants as it does to the ligand in a MOF.

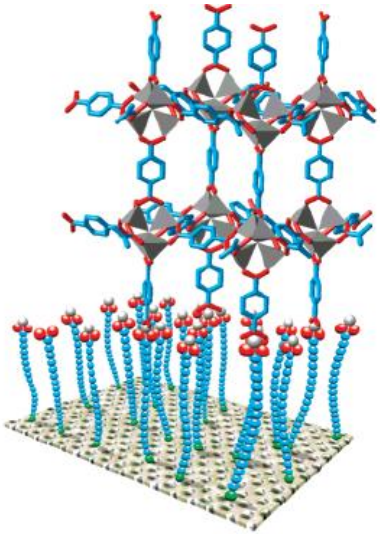

Figure 3. A simplified model of MOF-5 anchored to a carboxylic acid terminated SAM. [7]

When utilizing thiol-functionalized surfaces in the growth of SURMOFs, the solvothermal conditions under which a typical MOF synthesis is performed cannot be used, as the SAM/gold interface is quite fragile. For this purpose, new methods have been conceived.

A method to let crystals grow at lower temperatures is by aging the solution first, before immersing a SAM functionalized substrate into the solution. Both metal precursor and organic ligands are aged at a temperature of 75 $^{\circ}$C for at least three days after which the solution is heated to 105 °C for a very short moment to initiate crystallization. When a faint turbidity is detected, the solution will be filtered and rapidly cooled to room temperature and subsequently the SAM functionalized surface is immersed in the solution. Crystals will now start to grow in an oriented manner on the functionalized surface at room temperature (Figure 3). If the substrate is brought into contact with the aged precursor solution after a shorter aging time or at higher temperature, no oriented growth is observed.[20],[35] Although orientation can be controlled with this method, homogeneous distribution of MOFs on a substrate is harder to reach because growth is rather uncontrolled, leading to rough coatings consisting of large single crystals.[30]

The functional groups of SAMs can be used to mimic certain molecules which are present in bulk MOFs and this was published by Biemmi *et al.*[35] It was found that the orientation of growth of HKUST-1 [$Cu_3BTC_2(H_2O)_n$] (BTC = 1,3,5-benzenetricarboxylate) changes when functional groups of the SAMs were varied. Carboxylic acid terminated SAMs will behave as the BTC-linker in the MOF and -OH terminated SAMs are used to mimic the behavior of weakly bound water molecules; methyl terminated SAMs were used as an inert reference substrate. It was shown that films grew along the [100] direction when COOH-terminated organic monolayers were used, whereas the growth on OH-terminated SAMs was in the [111] direction. When a methylgroup was used, a faster growth process was noticed, but no particular orientation was found.

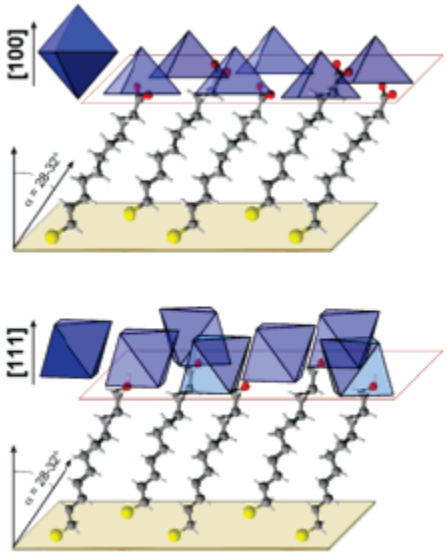

Figure 4. HKUST-1 crystals grow in the [100] direction on COOH-terminated SAMs (above), but in the [111] direction on OH-terminated groups (below). [17]

Another method to grow MOFs on substrates with high control over the orientation on SAMs, is by liquid-phase epitaxy (LPE) or layer-by-layer (LbL) growth process, which was first introduced by Shekhah *et al.*[36] for the synthesis of thin films of HKUST-1. Metal precursors and organic linkers in solution are added to the substrate separately in a step by step manner. After adding one component, the substrate is rinsed with a solvent to remove excess materials before the following component is added. The resulting thickness of a film is proportional to the amount of steps, since a new layer is produced with every cycle of steps. As described above, the growth direction of the crystals will highly depend on the terminal groups of the SAMs. However, the mechanics are not that well understood and a prediction of the growth direction is not easily made.

In an article published by Zacher *et al.*[19] it was shown that crystals can grow in unexpected orientations. A layer-by-layer synthesis of $Cu(ndc)(dabco)_{0.5}$ (ndc^{2-}=1,4-naphtalene dicarboxylate, dabco=1,4-diazabicyclo(2.2.2)octane) was performed on SAM modified substrates with a cycle of two steps; a copper acetate solution is added first, followed by ndc and dabco in a 1:1 ratio after rinsing the substrate. It was expected that with a pyridyl terminated SAM, crystals would grow in the [001] direction, since it mimics the dabco pillars. For carboxylic acid terminated SAMs it was expected that crystals would grow in the [100] direction, as this ligand will imitate ndc. The outcome of the experiments was rather surprising; crystals grown on pyridyl terminated SAMs do grow in the [001] direction, however, MOFs grown on carboxyl terminated SAMs gave an amorphous product. When the ratio of ndc:dabco was increased from 1:1 to 2:1, crystal growth was observed in the unexpected [001] direction. By changing the synthesis procedure from two steps to three steps, now adding ndc and dabco independently, more control over the growth orientation was accomplished. Excellent orientation in the expected [100] direction was obtained when ndc was added before dabco was introduced after a washing step. The reversed sequence resulted in a [100] orientation as well, although it was found to be less crystalline.

It can be stated that the functional groups of SAMs are of great influence on the growth direction of MOFs, but there are even more subtle characteristics within the SAMs that can have strong effects. It has been shown that the chain length of SAMs show a large effect on the growth direction of thin films of ZIF-8.[29] This is explained by the odd-even effect of SAMs; alkanethiols on gold are not completely aligned perpendicular to the gold surface, but are in fact tilted 30°. When the organic backbone of the surfactant has an even number of CH_2 groups the terminal methyl group is closer to a parallel orientation, in contrast to an odd number of CH_2 groups which leads to a more perpendicular orientation. (Figure 5)[37]

Depending on the number of CH_2 groups in the carbon chain and the fact that the organic backbones are not completely perpendicular to the surface, the methyl group at the end of the chain can have a different orientation. Most alkanethiols will have angles of 30°, making their methyl groups point upwards or sideways, determined by an odd or even amount of CH_2 groups.[37]

This effect was found to take place in the synthesis of thin films of ZIF-8, which was carried out on methyl terminated SAMs.[29] In this experiment, ZIF-8 was grown on patterned SAMs; with microcontact printing, small dots of alkanethiol assembled on a gold surface. The unfunctionalized surface was afterwards coated with 16-mercaptohexadecanoic acid for passivation. The substrate was then immersed in an aqueous solution of 2-methylimidazole, after which an aqueous solution of zinc acetate was slowly added. With the substrate on its side, ZIF-8 crystals started to grow on the surface. It was found that only oriented growth took place on alkanethiols (on a gold surface) with even numbered methyl chain lengths [$CH_3(CH_2)_nCH_2SH$, n = even].

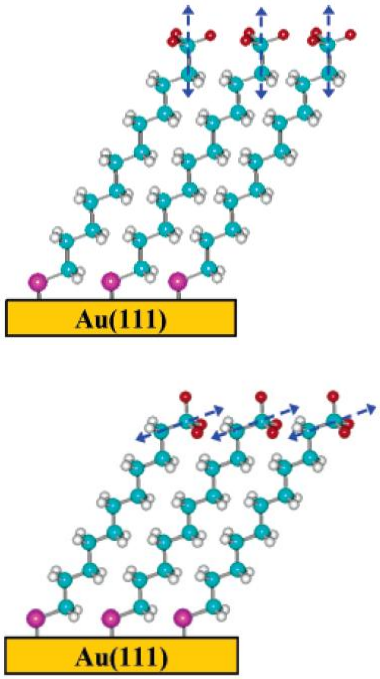

Figure 5. Terminal methyl groups of alkanethiols assembled on gold show a different orientation for an odd or even number of CH_2 groups.[37]

1.2.3 Aqueous room temperature syntheses

Syntheses of ZIFs have been mostly performed under solvothermal conditions in organic solvents, such as dimethylformamide (DMF).[13] However, Pan *et al.*[38],[39] have recently reported a method to synthesis ZIF-8 at room temperature in aqueous solutions. There are some advantages of performing hydrothermal syntheses over solvothermal syntheses. In the first place, no expensive and toxic organic solvents are used; the second advantage – which is of larger importance for this project – is that the conditions are much milder. This is convenient for growing ZIFs on SAMs, as SAMs will be able to withstand synthesis conditions at room temperature much better than at solvothermal conditions.

Although this may sound as an ideal synthesis procedure, this method does bring certain drawbacks with it. For the synthesis of single phase ZIF-8 crystals in aqueous solutions, a high concentration of precursors is needed and also a remarkably high ratio of 2-methylimidazole (HmIm) to zinc ions is

needed; a ratio of 70:1 (HmIm:Zn^{2+}) is required for optimum synthesis conditions. These reaction conditions will lead to a very low yield in terms of HmIm and a considerable loss of organic material, unless the uncoordinated HmIm are reused. The reason for the requirement of such high concentrations of HmIm in comparison to syntheses in organic solvents is thought to be caused by a higher pKa of HmIm in water than in organic solvents. Therefore it is expected that less imidazolates (mIm) will be present in aqueous solution, even if the same amount of HmIm is added to the different types of solutions. With less mIm available to coordinate to the zinc ions, other zinc complexes can form in the reaction mixture, such as zinc hydroxide or zinc nitrate hydroxide.[40]

It has been found that the concentration of HmIm can be reduced by adding triethylamine (TEA) to the solution. TEA is a weak base and will deprotonate HmIm before mixing it with the solution containing zinc ions and as result, it will initiate framework formation. Since there are now more deprotonated mIm linkers in the solution, there is a smaller chance of forming other zinc complexes. Owing to the basic properties of TEA, it is also able to deprotonate free Zinc-methylimidazolate complexes and commencing nucleation. By adding TEA in a 1:1 ratio to HmIm, the ratio of mIm:Zn^{2-} can be reduced to 16:1 to give satisfying results, although the BET surface area is reduced roughly by a half in comparison to the synthesis procedure described in the previous paragraph. [41] Hydrothermal syntheses of ZIFs with ligands other than HmIm were unsuccessful, it was hypothesized that a structure directing agent within the imidazole is necessary to grow zeolite like structures in water.

1.2.4 Self-assembled monolayers

Self-assembled monolayers (SAMs) have a functional headgroup that has a high affinity for the surface of the metal. Some surfactants have the ability to displace other organic molecules that were already adsorbed; the adsorbed molecules then adopt conformations that allow high degrees of van der Waals interactions with neighboring molecules to minimize their free energy. Together with the steric effects and hydrogen bonding between the surfactants, electrostatic and hydrophobic interactions, the adsorbed species can form (semi-)crystalline structures on the gold surface.

In the 1980s it was found that thiols readily adsorb and spontaneously self-assemble on the surface of gold.[42] Thiolates in solution react quickly with the surface and, within minutes, a dense coverage of thiolates is obtained from millimolar solutions. Soon after, a slow reorganization takes place that maximizes the density of adsorbates and minimizes the defects in the SAM. Some known experimental factors that are known to have an effect on the rate of formation are: the type of solvent, temperature, concentration of thiols, cleanliness of the substrate and chain length of the thiol.[37,43]

Thiols require activation of the S-H bond near the surface, before covalently binding to the gold. However, it is not known what happens to the hydrogen atoms after the thiol group reacts with the gold surface. Two probable explanations are that two hydrogens will form H_2 and leave the reaction mixture in the gas phase or that these hydrogen atoms react with oxygen in the solution to form water.

The choice of solvent is frequently ethanol, as it is capable of dissolving many types of thiols and moreover, it is inexpensive, available in high purity and it has a low toxicity. Hydrocarbon solvents are able to improve kinetics of formation, but they will most likely impede the organization of SAMs because of strong solvent-adsorbate interactions. *n*-alkanethiols do not dissolve well in polar liquids, but when polar solvents are used, the quantity of some defects is reduced and higher packing densities are reached.[44]

Organization of SAMs is mostly done at room temperature, but higher temperatures can increase the kinetics of formation and reduce defects in structures. The rate of desorption for other organic molecules adsorbed at the surface is higher at higher temperatures and reorganization is easier for thiolates.[45]

In this project, it was attempted to study the effect of functional groups of SAMs, of which imidazole is one. As imidazole terminated thiols are not commercially available, they have to be synthesized. A method to prepare imidazole terminated SAMs has been reported previously by Kisailus *et al.*[46] Starting with the adsorption of carboxylic acid terminated thiols on a gold surface, utilizing carbodiimide crosslinking chemistry, an imidazole terminated SAM is synthesized (Figure 6). Carboxylic acid reacts with 1-ethyl-3-(3-dimethylaminopropyl)-carbodiimide (EDC) to an unstable O-Acylicourea intermediate that is easily displaced by a nucleophilic attack from a primary amine. In principle, the reaction can be performed without using N-hydroysuccinimide (NHS). However, O-Acylicourea is easily hydrolyzed in the presence of water, resulting in the regeneration of the carboxyl. To increase efficiency, NHS is added to the solution. It will form a more stable NHS ester when coupled to the carboxyls. Then, histamine is added. The primary amine forms an amide bond with the original carboxyl group, and NHS is released into the solution again.[47]

Problems with this approach could be that the ketone can also be an anchoring point for the metals and that structure defects in the ordering of SAM layers will cause the ZIFs to grow in random orientations. The latter also occurred in the study by Li *et al*.[29] in which a perfect epitaxial match was present between ZIF-8 and the methyl groups of octadecanethiol SAMs on gold, resulting in an oriented growth. It was shown that it was not present for the 16-mercaptohexadecanoic acid SAMs, where also no oriented growth was observed.

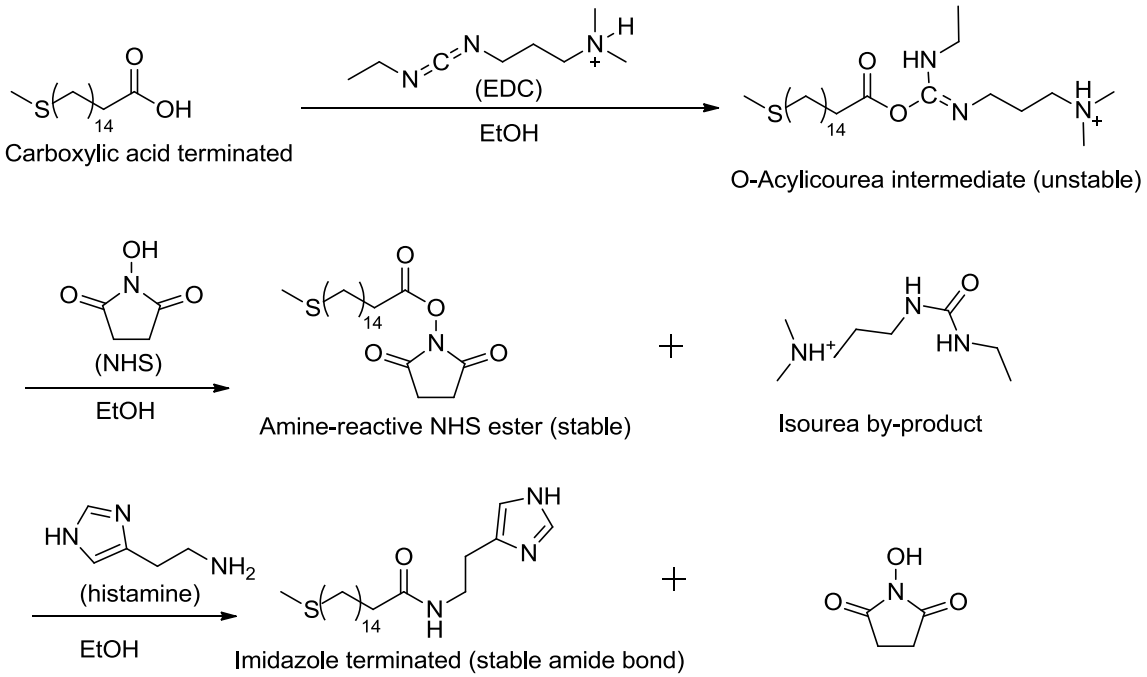

Figure 6. Synthesis of an imidazole terminated molecule, starting from a carboxylic acid terminated SAM.[47] EDC: 1-ethyl-3-(3-dimethylaminopropyl)-carbodiimide, NHS: N-hydroysuccinimide.

1.3 Methods

1.3.1 Materials

The following materials were used as received:

- Zinc nitrate tetrahydrate [$Zn(NO_3)_2.4H_2O$, Merck, 98.5%]
- Zinc nitrate hexahydrate [$Zn(NO_3)_2.6H_2O$, Sigma-Aldrich, ≥99%]
- Zinc acetate dihydrate [$Zn(O_2CCH_3)_2(H_2O)_2$, Sigma-Aldrich, >98%]
- 2-methylimidazole [HmIm, Sigma-Aldrich, 99%]
- Gold coated silicon wafer with a titanium adhesion layer [Ruhr-Universität Bochum]
- 16-Mercaptohexadecanoic acid [MHDA, Sigma-Aldrich, 99%]
- Octadecanethiol [ODT, Sigma-Aldrich, >98%]
- N-Hydroxysuccinimide [NHS, Brunschwig Chemie, ≥98%]
- 1-Ethyl-3-(3-dimethylaminopropyl)-carbodiimide [EDT, Brunschwig Chemie, ≥98%]
- Histamine dihydrochloride [Sigma-Aldrich, ≥99%]
- Chloroform [CH_3Cl, Interchema, Pract.]
- Dimethylformamide [DMF, ABCR, 99%]
- Ethanol [EtOH, Merck, 99.5% extra dry, absolute]
- Methanol [MeOH, Merck, for analysis]

1.3.2 Bulk syntheses

<u>ZIF-8 in DMF</u>

0.210g ($8.03*10^{-4}$ mol) $Zn(NO_3)_2.4H_2O$ and 0.060g ($7.31*10^{-4}$ mol) 2-methylimidazole were dissolved in 18 mL DMF in a 20 mL glass vial. The capped vial was heated at a rate of 5 ^oC/min to 140 ^oC in a programmable oven and kept at this temperature for 24 hours after which it was cooled with a rate of 0.4 ^oC/min to room temperature. The crystals were obtained by removing the mother liquor from the crystals by decanting and adding 15 mL chloroform. Crystals that were adsorbed to the glass were scratched off so that all the crystals could be vacuum filtrated and washed three times with DMF, after which they were dried in air at room temperature. [48]

<u>ZIF-8 in aqueous solution</u>

0.010g ($3.44*10^{-4}$ mol) $Zn(NO_3)_2.6H_2O$ was dissolved in 3 mL milli-Q water; 1.20g (0.0146 mol) 2-methylimidazole (mIm) was dissolved in 17 mL milli-Q water. The two solutions were mixed at room temperature in a glass vial and were shaken every 30 minutes. The resulting white precipitates were collected by two washing steps with water and centrifuging at 3000 RPM for 30 minutes. Then a washing step with methanol and centrifuging at 3000 RPM for 30 minutes was performed. The supernatant was removed and the particles were put in 3 mL methanol. The methanol was evaporated in air and dry particles were obtained. [49]

1.3.3 SAMs preparation

Carboxylic acid terminated SAMs

Gold coated silicon substrates of approximately 1 cm^2 were rinsed with ethanol and cleaned with a UV/ozone cleaner for 10 minutes after the ethanol had fully evaporated from the surface. They were then immediately rinsed with absolute ethanol. After rinsing with ethanol they were immersed in 2 mL 20 µM MHDA in 10 % v/v acetic acid: ethanol for 20-24 hours. The next day, they are washed intensively with ethanol, dried and stored under argon until used in further experiments.

Methyl terminated SAMs

Gold coated silicon substrates of approximately 1 cm^2 were rinsed with ethanol and cleaned with a UV/ozone cleaner for 10 minutes after drying in air. They were then immediately rinsed with absolute ethanol. After rinsing with ethanol they were immersed in 1 mM ethanolic solutions of octadecanethiol for 24 hours. The next day, they are washed intensively with ethanol, dried and stored under argon until used in further experiments.

Imidazole terminated SAMs

For this method, a solution of 5 mM EDC and 5 mM NHS in ethanol was used. The carboxyl functionalized gold coated substrate was dipped into this solution for 1 hour and rinsed with ethanol after that. Immediately after rinsing, it was immersed into 5 mM histamine in ethanol solution overnight and rinsed with ethanol.

1.3.4 Thin film syntheses

All reactions were performed with SAM functionalized gold coated substrates as prepared in section 1.3.3 and were carried out at room temperature. In the LbL syntheses, the solvents and solutions were introduced and taken off with a calibrated, automatic pump system.

ZIF-8 thin film synthesis on functionalized gold coated substrates in aqueous solution

A functionalized substrate was immersed in 4 mL of 1 M aqueous solution of 2-methylimidazole, with the SAMs facing down. Then, 0.2 mL of 0.3 M $Zn(O_2CCH_3)_2(H_2O)_2$ was added drop wise. Gold coated substrates were removed from the solution typically after 1 hour.[29] This method was tried with 10 times diluted concentrations as well; 4 mL of 0.1 M aqueous solution of 2-methylimidazole and 0.2 mL of 0.03 M $Zn(ac)_2$.

ZIF-8 Layer-By-Layer synthesis on functionalized gold coated substrates in aqueous solution

The LbL synthesis consists of 4 individual steps that are repeated 15-40 times in the following order:

1. 1.5 mL of 12.5 mM aqueous solution of $Zn(O_2CCH_3)_2{\cdot}2H_2O$ was added in 20 seconds to a functionalized substrate; the solution was removed after 10 minutes.
2. 1.5 mL milli-Q water was added in 20 seconds and removed after 10 minutes.
3. 1.5 mL of 25 mM 2-methylimidazole was added in 20 seconds to the substrate. The solution was removed after 10 minutes.
4. 1.5 mL milli-Q water was added in 20 seconds and removed after 10 minutes.[24]

ZIF-8 Layber-by-Layer synthesis on functionalized gold coated substrates in ethanol

The LbL synthesis consists of 4 individual steps that are repeated 40 times in the following order:

1. 1.5 mL of 1 mM $Zn(NO_3)\cdot 6H_2O$ in ethanol was added in 20 seconds to a functionalized substrate. The solution was removed after 10 minutes.
2. 1.5 mL ethanol was added and removed after 10 minutes.
3. 1.5 mL of 2.5 mM mIM in ethanol was added in 20 seconds to the substrate. The solution was removed after 10 minutes.
4. 1.5 mL ethanol was added in 20 seconds and removed after 10 minutes.

1.4 Results and discussion

1.4.1 Layer-by-layer synthesis

Thin films of ZIF-8 were grown on 16-mercaptohexadeconaic acid (MHDA) and octadecanethiol (ODT) as discussed in section 3.3.[24,29] After synthesis, the products were examined under an optical microscope. Thin films prepared on ODT and MHDA with a high concentration (1 M 2-methylimidazole, 0.3 M Zn(acetate)$_2$) showed almost a full coverage of the substrate with many cracks. With lower concentrations (0.1 M 2-methylimidazole, 0.03 M Zn(acetate)$_2$), small crystals were seen on the surface of the substrates and with the layer-by-layer method described in section 1.3.4, even smaller and more dispersed particles were observed.

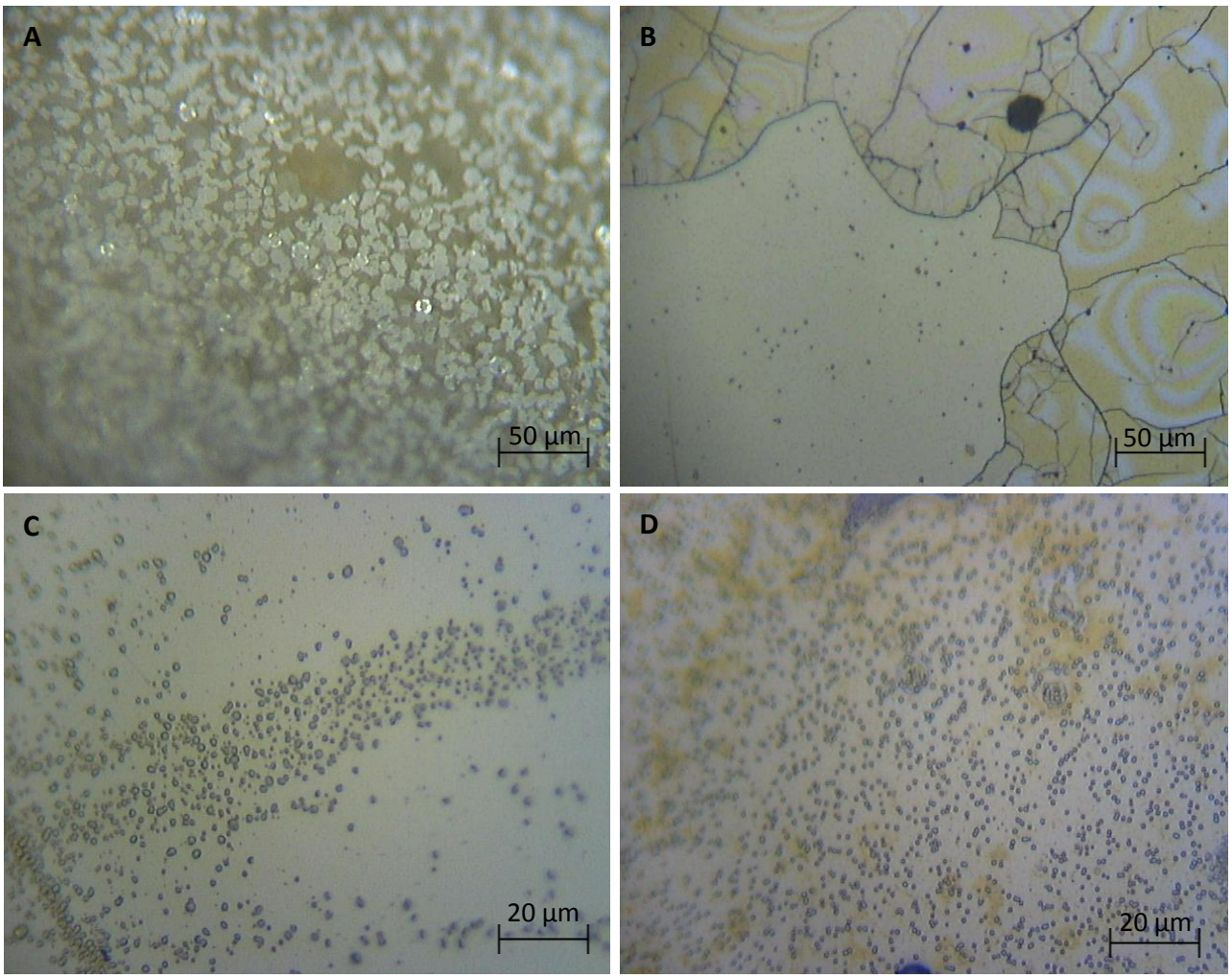

Figure 7. A) ZIF-8 crystals of around 5 µm synthesized under solvothermal conditions as described in section 3.1.
B) Edge of covered and uncovered ZIF-8 parts grown on MHDA synthesized by immersing MHDA functionalized gold coated substrate in high concentration of 2-methylimidazole and Zn(acetate)$_2$ solution.
C) Small ZIF-8 crystals on MHDA covered substrates, synthesized by immersing the MHDA functionalized gold coated substrate in a low concentration of 2-methylimidazole and Zn(acetate)$_2$ solution.
D) Small ZIF-8 crystals on MHDA covered substrates, synthesized by adding step-by-step 12.5 mM Zn(acetate)$_2$, ethanol, 25 mM 2-methylimidazole and ethanol for 40 cycles.

Raman spectra were measured and recorded between 3500-100 cm^{-1} on different parts of the surfaces of substrates. No signal was measured for parts of the gold coated surface on which no deposits were observed with the optical microscope. For parts where a deposition of material was observed, Raman spectra resembling that of bulk ZIF-8 was observed (Figure 8). However, small deviations from the bulk spectra were detected, the concerning assignment can be found in

Table 1. Differences in the spectra can be attributed to DMF (used as a solvent in the bulk synthesis) remaining in the pores after drying in air. Small shifts in energies are assumed to be an effect of the calibration of the lasers; for bulk particles a red laser with a wavelength of 785 nm was used and for SURZIFs a green laser was used with a wavelength of 532 nm.

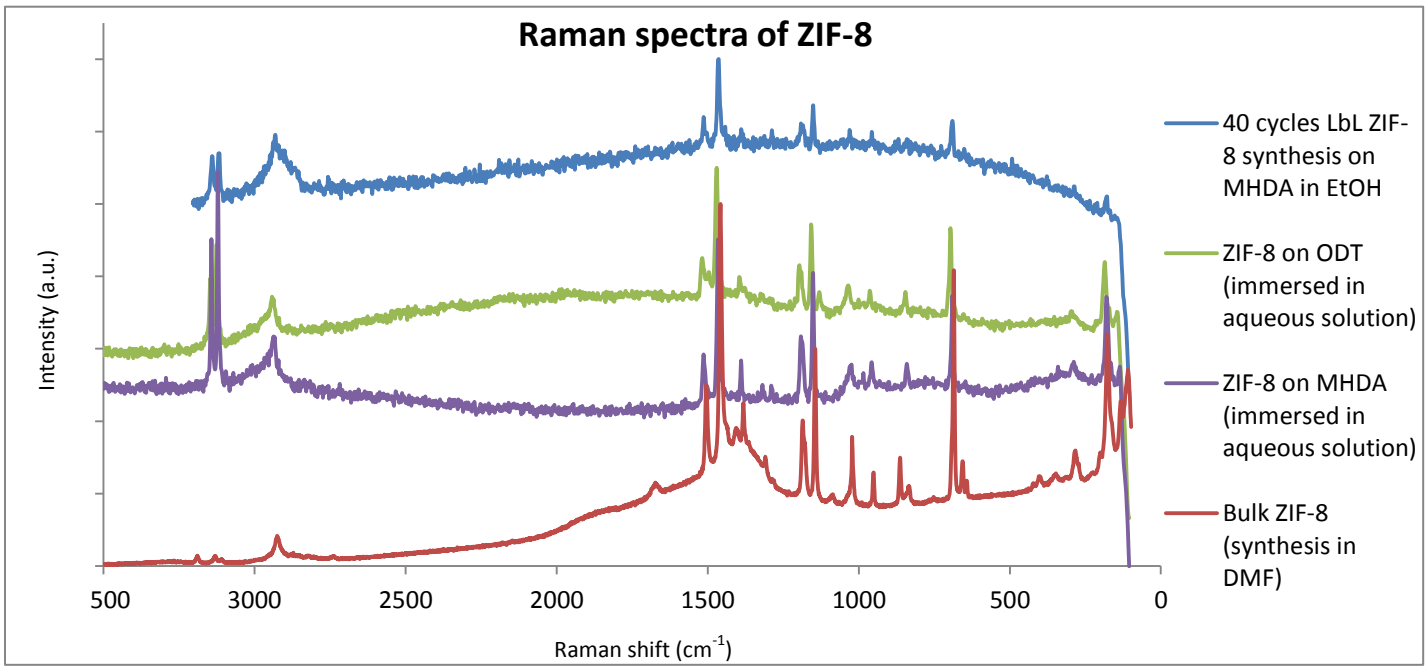

Figure 8. Raman spectra of a ZIF-8 crystal synthesized by a 40 cycle LbL synthesis on MHDA (blue), thin film of ZIF-8 on ODT (green), thin film of ZIF-8 on MHDA (purple) and ZIF-8 synthesized in solvothermal conditions.

Table 1. Peak assignment of selection of peaks from the Raman spectra pictured in Figure 8.[50]

Thin film ZIF-8	Bulk ZIF-8 (solvothermal)	Assigned to
3170	3179	=C-H stretch
3116	3110	=C-H stretch
2930	2919	-C-H stretch
-	1672	C=O stretch
1511	1509	N=C-N stretch
1470	1468	Ring stretch
1389	1387	Ring stretch
-	862	Stretch C-N
697	695	In plane bending ring
-	655	Deformation O=C-N

Although no XRD measurements were performed on the SURZIFs, results from Raman spectroscopy suggest that deposition of ZIF-8 on MHDA and ODT functionalized surfaces had taken place in every synthesis method. However, when 40 cycles of the LbL method was applied or when using a lower concentration of Zn^{2+} and HmIM in the direct synthesis, no full coverage of the gold coated substrates were observed. For this reason, the particle sizes of the SURZIFs were measured with Atomic Force Microscopy (AFM), of which a profiling picture is illustrated in Figure 9. A film thickness of about 20 nm was expected after 40 cycles of LbL. However, this did not correspond with the result: larger particles showed heights of up to 100 nm, but most particles had a height in the range of 30-40 nm. Therefore it was hypothesized that the washing step does not wash away all the precursors. Since there was no full coverage of SURZIFs on the surface, it was thought that the initial coverage of SAMs was low as well.

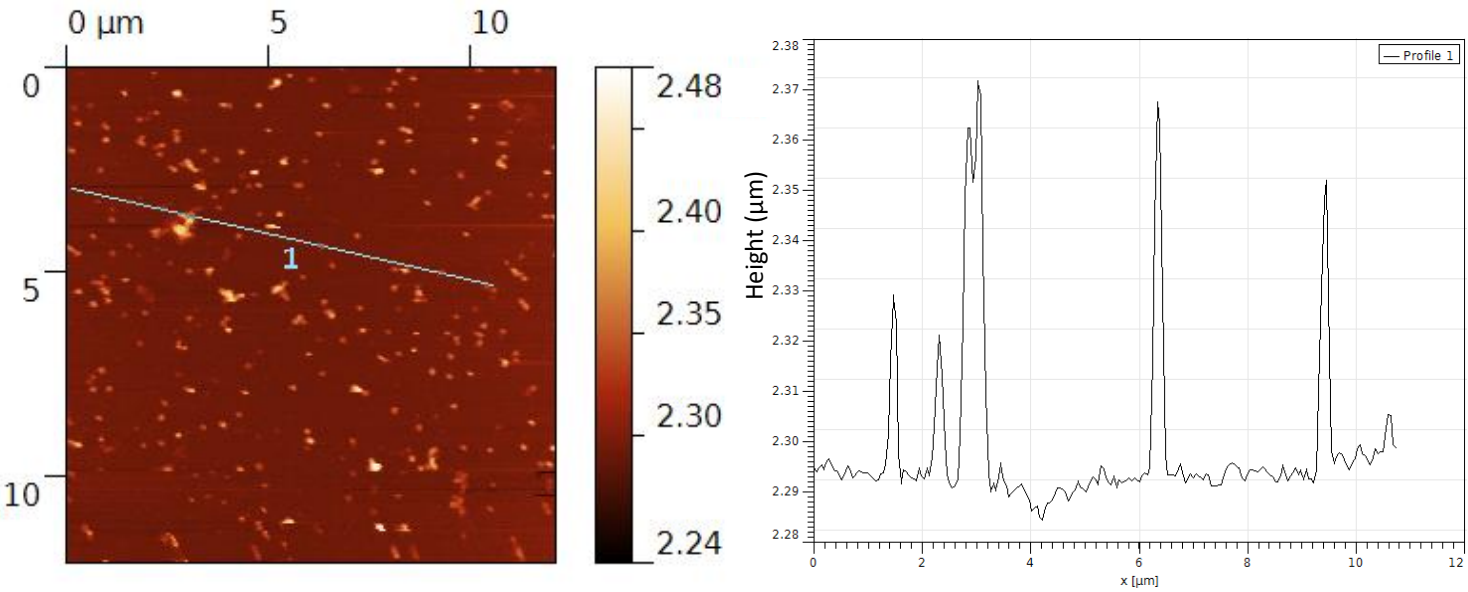

Figure 9. Left picture: height image; right picture: profiling picture along the blue line in the height image.

1.4.2 Self-Assembled Monolayers

Multiple techniques were used to study substrates that were immersed in solutions with thiols to measure if the deposition of thiols had taken place. Contact angle measurements can give a relatively fast answer to which functional groups are present at the surface and their homogeneity.

The results obtained using contact angle measurements were not only inconsistent between the samples, but also within most samples, as illustrated in Figure 10. Contact angles could vary between 20° and 80° and measurements carried out on unfunctionalized substrates were inconsistent as well, which gave reason to believe

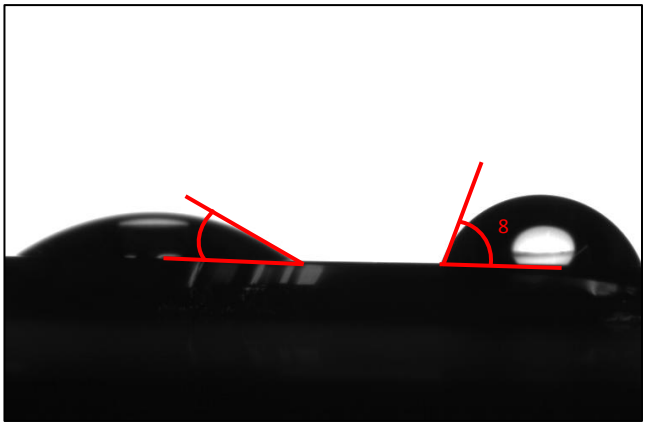

Figure 10. Contact angle measurements on a single gold coated substrate functionalized with MHDA.

that the gold coated substrates were not of high enough quality for the self-assembly of MHDA.

In contrast to the unfunctionalized gold coated substrates and the MHDA functionalized substrates, substrates coated with ODT did show a significantly higher and more homogeneous contact angle over the samples with an average of 97±8.5. Although it is not in full agreement with other published work[51], it does show a higher contact angle. Contact angles also highly depend on the structure/quality of the SAMs and possible pollutions on the surface, making it hard to directly compare the results with other publications.[52]

For a more qualitative analysis of the surfactants, grazing angle IR was used. At an incident angle of 86° a spectrum was obtained that showed 2 relative intense peaks at 1450 cm^{-1} and 1570 cm^{-1}. These peaks are associated with carboxylates, which is not expected after washing with a solution containing 10 % v/v acetic acid. In fact, the washing step with addition of acetic acid was performed to prevent the formation of carboxylates on the SAMs, as described by Wöll *et al.*[53] For this reason, two additional measurements were performed on an MHDA functionalized substrate and an unfunctionalized substrate washed with absolute ethanol and subsequently with 10 % acetic acid. The two peaks were only visible in the spectra measured after washing the substrates with 10% acetic acid, and are assigned to the asymmetric (1570 cm^{-1}) and symmetric stretching (1450 cm^{-1}) of the carboxylates of adsorbed acetic acid. In the spectra of MHDA functionalized substrates. Peaks are also observed at 3000 and 2937 cm^{-1} and are associated with C-H stretches. This indicates that there is at least some deposition of organic material. No spectra were obtained for ODT SAMs.

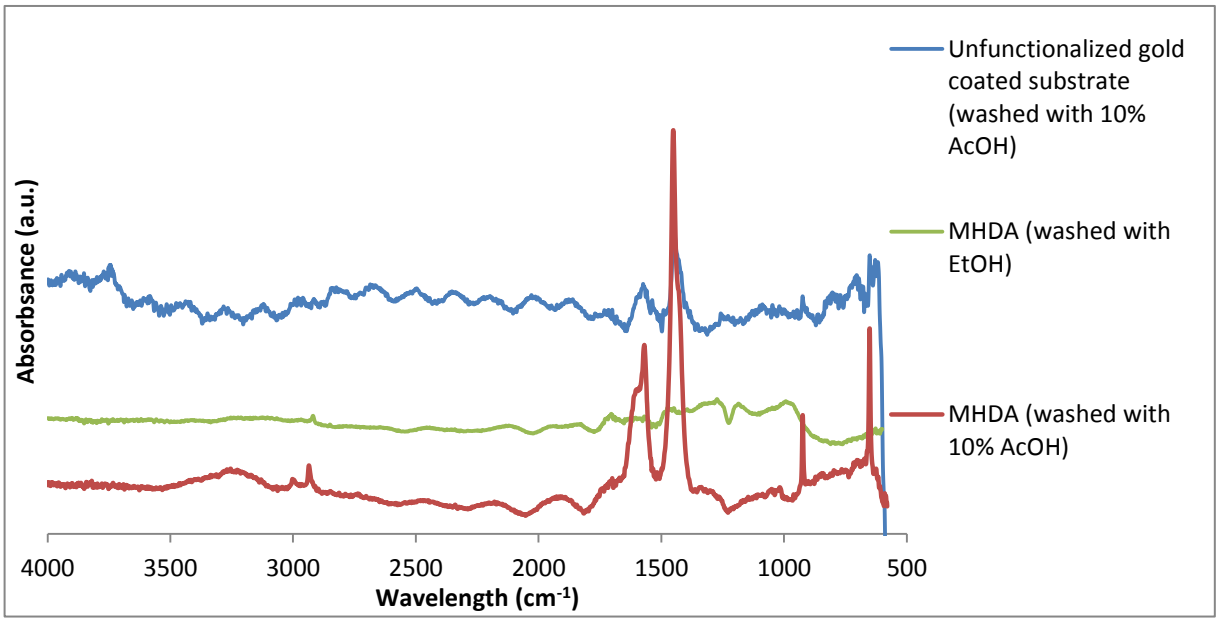

Figure 11. IR spectra of a gold coated silicon wafer and after immersion in a solution containing 25 µM 16-mercaptohexadecanoic acid (MHDA) in 90:10 ethanol:acetic acid. The substrates were subsequently washed with ethanol or 90:10 ethanol:acid (v/v).

AFM was used to measure the coverage of SAMs on gold coated surfaces. In the phase images shown in Figure 12 it can clearly be seen that ODT has a partial coverage over the surface. It is not known what the coverage of MHDA is on the gold coated surface, since the images obtained with AFM were blurry. This can be a result of a positive interaction between the carboxylic acids and the AFM tip or the presence of unbound organic surfactants or other organic material on the surface that are carried away with the tip.

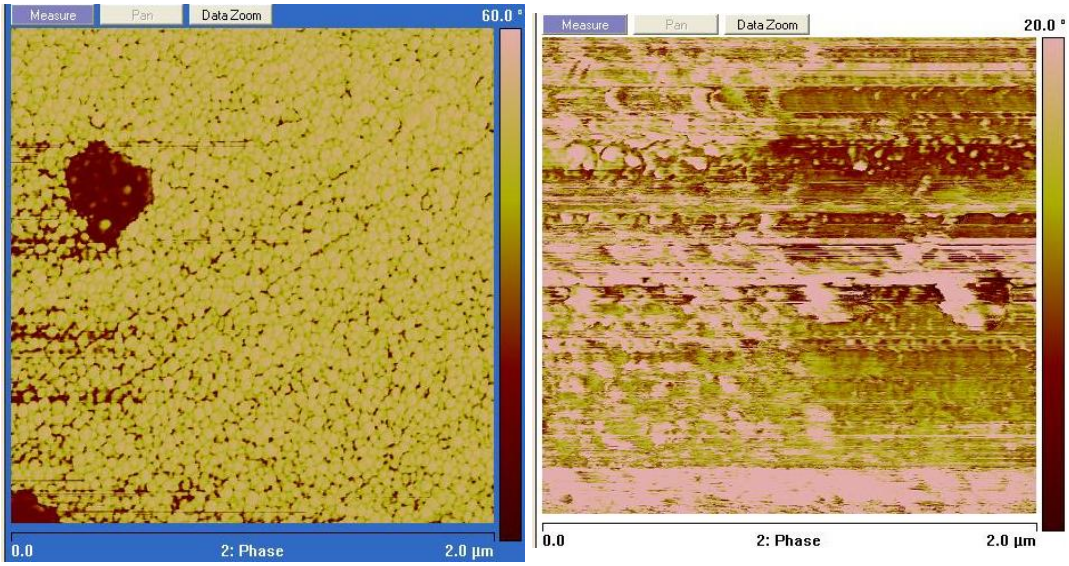

Figure 12. Phase images of self-assembled ODT (left) and MHDA on gold coated silicon wafers, the images are a representative part of the sample, 2 µm by 2 µm in size. The scale bar for the phase shift in the left image is 0° to 60°, and the phase shift for the right image is 0° to 20°

1.4.3 Quality of gold coated substrates

Since the coverage of ODT SAMs was low and it was unknown for MHDA, additional measurements were performed on unfunctionalized gold coated silicon wafers, as the quality of the gold is of great importance. AFM measurements were performed on the substrates to evaluate the height differences in the sample of which one example is depicted in Figure 13. In this example, it becomes very clear that the sample is not atomically flat at all; instead it consists of many gold nanoparticles of around 20 nm. A rational explanation is that a rough surface such as depicted in Figure 13 will cause problems in the self-assembly of thiols.

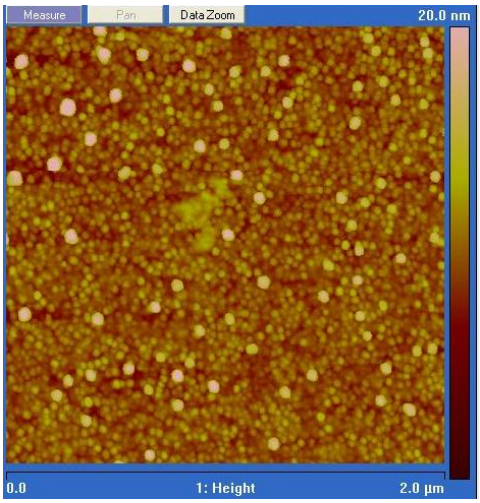

Figure 13. Height image of a gold coated silicon wafer supplied by Ruhr-Universität Bochum. The image is a representative part of the substrate, 2 µm by 2 µm; the scale bar depicts the height difference in color from 0 nm to 20 nm.

To improve quality and reduce the roughness, the gold coated wafers were hydrogen flame annealed, which is a widely used method to obtain more atomically flat surfaces.[54] This method did not yield a more flat surface

in the experiments, but instead ruined the gold surface and exposed silicon. Therefore, annealing in an oven at 250 °C was carried out over 3 hours.[44] This method resulted in the formation of larger terraces that showed more invariable heights per terrace (Figure 14).

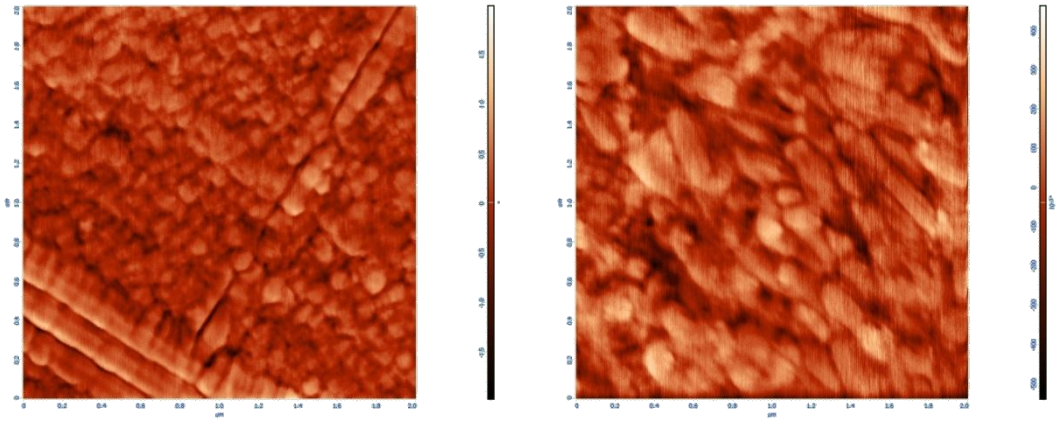

Figure 14. AFM phase images of gold coated substrate (left) and the same surface after annealing in air at 250 °C for 3 hours. The images are 2 µm by 2 µm and are a representative part of the substrate.

Although the substrates were flatter than before after annealing in the oven, no increase in the coverage of the surface with MHDA or ODT SAMs was observed with grazing angle FTIR.

1.5 Conclusions

By applying the methods as described in section 1.3.4, ZIF-8 solid depositions were prepared on gold surfaces, although no homogeneous thin films were obtained. Depositions were characterized with AFM, optical microscopy and Raman spectroscopy.

Since it was thought that the lack of homogeneity was caused by a bad SAM quality, the substrates were characterized with AFM and grazing angle IR. Since the AFM images gave a blurry result, no conclusion about the quality of MHDA SAMs could be drawn with this technique. For ODT SAMs, low coverage was observed. Very weak bands were observed in the grazing angle IR spectra of MHDA SAM that were associated with C-H stretches, but the characteristic bands for carboxylic acid bands were not measured. This can be a result of a low thiol coverage due to improper sample preparation, or an improper use of the instrument. Additionally, inconsistent results were obtained with contact angle measurements. To sum up, it was concluded that no full coverage of the gold coated substrates has been achieved.

AFM images showed that the surface of the gold coated substrates consists of 20 nm gold nanoparticles. It was hypothesized that a rough surface will make it very difficult for the thiols to form a well-defined SAM.

1.6 Outlook

To improve the formation of high quality SAMs, better quality gold coated substrates have to be used. Additionally, since it has been shown with AFM that there are adsorbed species on the surface, the grazing angle IR technique has to be improved as well to be able to measure the SAMs. An interesting technique to characterize the SAMs is Chemical Force Microscopy (CFM).[22] By chemically modifying the tip, it is possible to measure the type of functional group present on the surface of the substrate.

Once there is a control over the formation of SAMs and these products can be characterized with the use of grazing angle IR, AFM and CFM, it will give rise to more interesting properties. The ultimate goal would be to introduce varying functional groups to the SAMs by using carbodiimide crosslinking chemistry. With the above mentioned characterization techniques and XRD different growth orientations of SURZIFs can then be directly linked to changes in the functional groups.

Chapter 2

POST-SYNTHETIC CATION EXCHANGE IN ZIF-8

2.1 Introduction

Within our modern society there are virtually no materials made by mankind without the use of catalysts. Ranging from the plastic bags at the supermarket to the fuels of our cars, all kinds of materials are prepared from what was originally crude oil.

Catalysts are not only used in industry for the synthesis of products that can help people make their life's simpler and easier. They come in a multitude of forms, which are categorized in 3 subdisciplines in catalysis: bio-catalysis, homogeneous catalysis and heterogeneous catalysis. An obvious example of the subdiscipline bio-catalysis is the function of enzymes in organisms; within bodies and cells they increase reaction rates for reactions which are crucial for the lives of the concerning organisms. Enzymes are often very specific for one type of substrate and will lead to only one specific product. Although biocatalysts are highly selective and active for certain reactions, they cannot be used for many industrial applications since they decompose quickly under harsh conditions, such as high temperature or pressure.[55]

The second subdiscipline – homogeneous catalysis – covers systems in which reactants and catalysts are in the same phase. Homogeneous catalysts are often very active and are used in many reactions, for instance in the synthesis of plastics. Reaction mechanisms of homogeneous catalysts are in general reasonably well understood, leading to high control over the selectivities. A downside of using homogeneous catalysts is that they are hard to separate, because they are often also in the same phase as the product. The third subdiscipline is heterogeneous catalysis, which means that the catalyst and the reactants or not in the same phase; usually referring to solid catalysts and gaseous or liquid reactants.[55]

The third subdiscipline – heterogeneous catalysis – has one big advantage over homogeneous catalysis: the catalyst is easier to separate from the products, since catalysts and reactants are in a different phase. A disadvantage of heterogeneous catalysts is that they have a volume of which only the surface acts as a catalyst. The particles are often made as small as possible (nanometers) and are bound to a support material to keep them dispersed and to prevent aggregation. A porous support is often chosen since it has a higher surface area than bulk material. Furthermore, by tuning pore sizes, size-selective catalysis can take place. Because there are many possible (simultaneous) reactions occurring at the surface of the catalyst and the support, the reaction mechanisms are not as well understood as they are for homogeneous catalysts. This often leads to a lower control of the selectivities.[55]

Since both homogeneous and heterogeneous catalysis show distinct advantages over each other, a logical thought would be to combine both types of catalysis one way or another. Different methods have been designed to 'heterogenize' homogeneous catalyst; by capsulation[56], anchoring to a surface[57] or with use of polymer nanoreactors.[58]

Metal Organic Frameworks (MOFs) and Zeolitic Imidazolate Frameworks (ZIFs) can be of great importance to the concept of heterogenizing homogeneous catalysts. In fact, they can be seen as heterogenized homogeneous catalyst themselves; they consist of many soluble secondary building units (SBU) that bind to each other and will crystallize under the right reaction conditions. With the

abundance of choice in the many different linkers and metals, a large amount of alternative functionalities can be given to a MOF.

Although there are multiple methods invented to functionalize a MOF for catalytic reactions,[59] the easiest one would be to prepare a MOF with catalytic activities in the metal nodes or linkers already. However, the freedom of choice of the metals for ZIFs is rather limited, since examples of ZIFs with metals other than cobalt or zinc are scarce.[12] For instance, ZIFs prepared from iron cations are known[60], but despite its high thermal and chemical stability, the framework collapses upon removal of the guest molecules in the pores. In the pores of the material, ferrocene molecules are present, giving stability to the framework.

As an alternative to the direct synthesis of MOFs or ZIFs with the desired metal precursor, a new method has been conceived to change the metals in the ZIFs by post-synthetic exchange (PSE). PSE relies on the fact that metal nodes and linkers within MOFs are not statically fixed in their place. It has been found that metals in even the most robust and inert MOFs can be exchanged with metal ions from solution and more surprisingly: solid isostructural MOFs are even capable of exchanging metals and linkers through the solution without ever being in direct physical contact.[61] During and after the exchange process, the MOFs have retained their initial structure.[62] Even when organic bridging ligands with different sizes are introduced to the framework, the MOFs retain their structure. Li *et al.* showed that longer organic ligands can be added stepwise, without losing the framework structure. With XRD they showed that the framework structure was retained and that only the peaks shifted to lower 2θ when longer ligands were inserted.

The feature of exchanging metal ions/linkers from the framework with cations/linkers from the solution has been found to also take place in ZIF-8 and ZIF-71 in more recently published articles.[1,63]

PSE is a very promising approach to functionalize MOFs and ZIFs because new metal cations or linkers can be introduced to the structure without changing or destroying the crystal structure. The interesting part of PSE is that with this method, species can be incorporated in the framework that would otherwise not be included in the framework or would lead to a drastically different structure. Since the amount of metals and linkers that one can use to form a framework is expanding significantly by using PSE, research in this field could lead to many new types of ZIFs and MOFs. Many different functionalities and active metals can be inserted into the framework, leading to possibly higher active and selective catalysts. Besides creating new types of ZIFs and MOFs, PSE can provide additional insights in the chemical dynamics between linkers, metals and SBUs.

A possible interesting candidate for proving the concept of creating a catalytic active ZIF with sieving effect is by inserting manganese cations into ZIF-8 particles. ZIF-8 is a very stable type of MOF; they are able to retain their structure in boiling water, methanol or benzene.[13] ZIF-8 is a fairly easily synthesized ZIF; built up from zinc metal nodes and 2-methylimidazolate linkers, it forms spontaneously in water and alcohols at room temperature.[41,64]

ZIF-8 is not expected to have a high catalytic activity in (ep)oxidation reactions since the zinc(II) complexes in the framework have full d^{10} orbitals. However, if manganese could be introduced to this framework, it could possibly be a very interesting heterogeneous catalyst, because manganese is

known to be an excellent (ep)oxidation catalyst for homogeneous reactions[65] and heterogenized versions.[66] Besides being a very well-known catalyst for epoxidation reactions, manganese is not a very expensive material as it is the 12th most abundant material, making up for about 0.1% of the total amount of atoms in the earth's crust.[67]

This chapter will focus on the synthesis and the post-synthetic cation exchange (PScE) of ZIF-8 with manganese. It was tried to reproduce the method that was previously described by Fei *et al*.[1] This exchanged material is then applied as a catalyst in chapter 3.

2.2 Theory

2.2.1 Post-synthetic Cation Exchange

ZIFs are usually prepared with zinc or cobalt cations, although a few other ZIFs are known that have been synthesized with lithium, copper, manganese and cadmium cations.[12] In principle, it is possible to control the structure of the ZIFs by selecting organic linkers and metal cations, however, it has been found to be difficult to prepare ZIFs with metals other than zinc or cobalt and to obtain materials with identical structures.

Recently, a new method has been developed which makes use of the fact that metal nodes in the MOF crystals are in equilibrium with metal cations in the solvent. New metal cations can be introduced to the crystals in relatively mild conditions, by exchanging them from the solution with the metal nodes in the crystals; this is called post-synthetic cation exchange (PScE). [62,68,69] It is possible to reversibly exchange all the original metals of the MOFs by new metals without destroying or altering the initial structural integrity and even single crystallinity.

This method has not only been used on instable MOFs, but it has also been used to insert new metals with the existing metals in 'inert' MOFs and it was found that even ZIF-8 and ZIF-71 are able to exchange their metals.[1] For ZIFs, it was found that 10 to 20 percent of zinc could be replaced by manganese by immersing the ZIFs (0.2 mmol equivalent of zinc) in 5 mL methanol containing 0.6 mmol (0.12 M) dissolved manganese.

There are multiple conditions that have effect on the rate and succession of PScE. One rather obvious parameter is the total time that is used to soak the MOFs in the precursor solution. It has been found that the total amount of exchanged metal is increased over time. However, the exchanged metals are not homogeneously distributed; it was observed that exchange first happens selectively in the outer shell of the particle, leading to a core-shell hetero structure. With increasing incubation time, the amount of exchanged metal nodes increased until a full exchange was observed for the flexible framework PMOF-2. The selectivity for exchanging the outer shell first was explained by a variation of flexibility in the framework. It was suggested that the framework is more flexible in the outer parts than it is in the middle of the crystal.[70] Although it seems logical that flexible frameworks exchange faster than rigid frameworks, a simpler explanation for finding this distribution would be that it plainly takes time for the metal ions to diffuse through the pores.

The concentration of metal precursors in solution should exceed the total amount of metal in the nodes of the immersed frameworks by a large amount to assure exchange. When concentrations are too low, no exchange will take place, but the metals will instead only physisorb to the surface of the MOF. Physisorbed cations are easily removed from the framework in solvents and are not desired, since solid catalysts are wanted. [71] The particle size appeared to be an important factor in the exchange method as well; after grinding zinc based MOFs, it was found that the particles preferred to adsorb almost exclusively Pb^{2+}, while larger particles preferred to exchange mostly Cd^{2+} ions when multiple cations were present in solution.[72]

Methanol is often chosen as the solvent for metal exchange, as it gives higher exchange rates than DMF[70], acetone or other alcohols[73]. Water has not been used as a solvent as most MOFs are not stable in aqueous solutions. An explanation for the higher exchange rates in methanol compared to other solvents, is that methanol is a smaller molecule and will therefore form smaller hydration shell around the dissolved metals and counter ions. This allows faster diffusion and closer interaction with the framework.[74] It is thus expected that water will have even a more positive effect on the exchange rates for non-hydrophobic MOFs, although care should be taken with respect to the framework stabilities in aqueous solutions.

Although the effect of pH on the exchange process has not been studied yet, it is expected that it has a large influence. First and foremost, stabilities of MOFs and ZIFs are highly dependent on the acidity of the solution. [75,76] When the pH decreases, the carboxylic or imidazolate linker will get protonated while at high pH the metal will get hydroxylated; both will lead to a disruption of the framework. As a result of changing framework stabilities at different acidities, it is hypothesized that exchanging at a higher or lower pH will make the process more facile than at neutral conditions. An analogy to zeolites can be made; the pH of the solution should be optimized to increase the metal loading during ion exchange or electrostatic adsorption.[77] A common method to apply strong electrostatic adsorption is to first determine the point of zero charge of the material, followed by a metal uptake while measuring the pH. For ZIFs it is expected that a higher pH will lead to higher adsorption of metal cations since the surface is more likely to be negative, thus leading to higher electrostatic interactions. [25]

Differences in the exchange rate caused by the use of various metal complexes are expected as well. Some coordinating ligands will have a stronger interaction with metals than others. For instance, bidentate ligands such as acetylacetonates will have stronger interactions than most monodentate ligands. Also, bonds between halides and metals are weaker than for most monodentate ligands since large ionic radii will make up weak bonds.[78] It is expected that precursors with weaker interacting ligands will lead to a higher rate of exchange and this has indeed been published.[69]

2.2.2 Stabilities and preferred geometries

The Irving-Williams series refer to the relative stabilities of metal complexes and the following order has been found:

$$Ba^{2+} < Sr^{2+} < Ca^{2+} < Mg^{2+} < Mn^{2+} < Fe^{2+} < Co^{2+} < Ni^{2+} < Cu^{2+} > Zn^{2+}$$ [79]

Besides electrostatic effects that have effect on the stability of the complexes, ligand-field stabilization energies (LFSE) are of great importance for the higher stabilities of metal complexes from iron(II) to zinc(II). Strong-field ligands cause a low spin orientation of the electrons in the d-orbitals and therefore the additional stabilization can be explained by the ligand-field stabilization energies (LFSE). Zinc(II) has a lower binding energy than copper and nickel; it has no benefit from LFSE since it contains 10 electrons in the d-orbitals.

The Irving-Williams series for a select group of metal-imidazolate complexes is illustrated in Graph 1. From this graph can be clearly seen that cobalt(II) and zinc(II) complexes have almost identical formation constants, and log K_1 values of respectively 2.46 and 2.55.[80] This could possibly be a reason why there are many more ZIFs known that are prepared from zinc and cobalt than from any other metal; the stability of the complexes is in the preferred range for a rigid formation, but there is still some flexibility for rearrangement to the kinetically favored ZIF crystal.

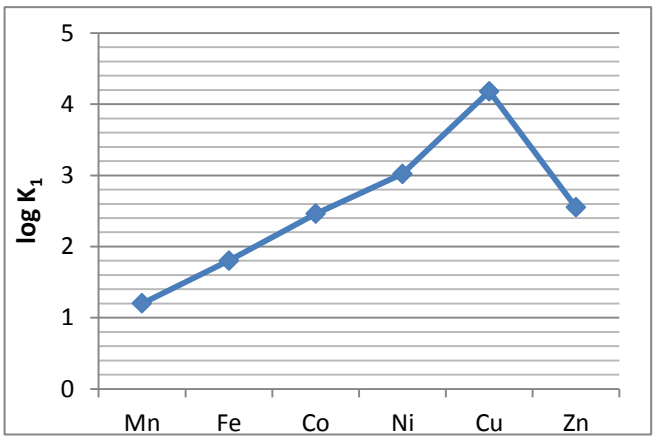

Graph 1. The variation of formation constants K_1 for a group of M^{2+} imidazolate complexes. The values for the K_1 constants are taken from a publication on metal-imidazolate complexes. [80]

Zinc(II) complexes prefer a tetrahedral coordination as they have full d-orbitals and therefore tetrahedral coordination geometries will lead to a lower energy state than that octahedral geometries would lead to. Manganese(II) complexes on the other hand have a d^5 composition. With a high field ligand, such as 2-methylimidazole, the ion prefers to be in a low spin configuration, increasing the preference of $Mn(mIm)_2$ complexes to octahedral geometries. With 5 electrons in the t_{2g} orbital, the complex optimizes its LFSE. It is believed that the direct synthesis of an isostructural ZIF-8 with manganese ions will therefore be impossible because it will not show the same geometries as $Zn(mIm)_2$ complexes.

It is not exactly known how manganese cations will behave when they are exchanged with the zinc ions in ZIF-8. Will they form tetrahedral coordination geometries, causing them to be in a higher energy state or will they bind to mIm octahedrally without destroying the crystalline structure? If the latter is the case, manganese ions introduced to the ZIF-8 crystal by the PScE method exhibit free – possibly catalytically active – sites, where the free sites are coordinated by weakly bound solvent molecules. A third possibility is that manganese will increase the strain on the framework as it prefers octahedral geometry; this could lead to a disruption of the framework.

Since manganese has a larger ionic radius than zinc in both octahedral (low-spin) and tetrahedral (high-spin) geometries – 0.67 and 0.66 Å respectively versus a radius of 0.6 Å for zinc in ZIF-8 – a small shift in the XRD pattern to lower 2θ angles is expected. It cannot be said with certainty that this effect will be noticeable when manganese is randomly incorporated. If this is the case, the peak intensities should decrease.

A technique which could give information on the types of nitrogen, zinc and manganese present in the exchanged ZIF-8, is X-ray photoelectron spectroscopy (XPS). XPS is a surface sensitive technique and will only give information of maximum the outer 10 nm of the material (section 4.9). With TGA, the thermal stability of the ZIF-8 can be measured and could give a clue about the stability of the framework and whether there are any solvent bound molecules present in the pores. With N_2 physisorption the (BET) surface area can be measured and as a result it can tell something about molecules present in the pores.

2.3 Methods

2.3.1 Materials

The following materials were used as received:

- Manganese acetylacetonate [Mn(acac)2, Sigma, purity not specified]
- Manganese nitrate hexahydrate [$Mn(NO_3)_2.6H_2O$, Sigma-Aldrich, >97 %]
- Manganese chloride tetrahydrate [$MnCl_2.4H_2O$, Sigma-Aldrich, >98 %]
- Nitric Acid [HNO_3, Merck, 65%]
- Sodium hydroxide [NaOH, Merck, 99%]
- Hydrochloric acid [HCl, Merck, 37%]
- 2-methylimidazole [HmIm, Sigma-Aldrich, 99 %]
- Methanol [Interchema, Pract.]

2.3.2 ZIF-8 synthesis in methanol

0.63 g $Zn(NO_3)_2.6H_2O$ is dissolved in 30 mL methanol and is added to 0.66 g 2-methylimidazole in 30 mL methanol. The mixture is stirred and left to stand for one day. After 24 hours, the particles are collected by centrifuging at 3000 RPM for 10 minutes. Then, they are washed two times with 25 mL methanol and are recollected by centrifuging at 3000 RPM for 10 minutes again. After washing, the particles are dried overnight at room temperature in air. The particles are further dried by placing them in an oven at 65 °C for 3 hours.[64]

2.3.3 Post-synthetic cation exchange

The manganese is introduced to the framework as previously reported by Fei *et al.*[1] with some adjustments. In this procedure, 90 mg of dried ZIF-8 (equivalent of 0.4 mmol zinc) is immersed in 10 mL methanol solution, containing 0.12 M of different manganese complexes. Three different kinds of manganese(II) precursors were used, namely, $Mn(NO)_3.6H_2O$, $Mn(Acac)_2$, and $Mn(Cl)_2.4H_2O$. After the acidity of the mixture was increased or lowered to the desired pH for the exchange process, the mixture was incubated at 55 °C in a preheated oven for 24 hours. When the particles were cooled down to room temperature, the mixture was centrifuged and the supernatant was removed. The (brown) particles were washed twice with 25 mL methanol and were recovered with centrifugation for 10 minutes at 3000 rpm. When the solvent was no longer colored, the particles were left to soak in methanol for three days. Twice a day the solvent was replaced with fresh methanol. After three days, the particles were centrifuged and the supernatant was removed, they were then dried at 65°C for 3 hours.

2.4 Results and Discussion

2.4.1 Metal concentration

After the synthesis and exchange methods, the now brown colored particles were first analyzed with powder XRD to see if the crystal structure was retained; an example is shown in Figure 15. This figure shows that ZIF-8 synthesized in methanol is isostructural to ZIF-8 synthesized in DMF, and more importantly, ZIF-8 does not change structure after exchanging the zinc metal nodes with manganese.

A small shift to smaller angles is seen in the diffraction pattern after 19% of the original zinc content is replaced with manganese, as is expected when zinc is replaced by larger manganese ions (an ionic radius of respectively 0.6 and 0.66 Å). However, this effect can also be credited to an inconsistency of the stage height, caused by the use of a different sample holder or a slight change in the amount of sample used for each measurement. Indeed, with different samples, peaks were shifted to higher or lower angles, irrespective of the amount of manganese present in the particles.

To measure shifts in the diffraction patterns, the difference in peak positions for all samples at a 2θ of around 8.9° 21.2° and 35.0° were therefore compared, but no significant change was observed for the samples after exchanging. A final XRD experiment with a mixed powder of ZIF-8 with ZIF-8 [$Zn_{0.81}Mn_{0.19}$] showed no multiplets in the diffraction pattern, indicating that truly no shift has taken place. As there were no shifts observed and the noise increased by a small amount, this characterization technique could not give decisive answer to whether or not the manganese has truly replaced zinc in the framework.

To determine the amount of manganese incorporated into the framework, measurements were performed with AAS, ICP-OES, EDX and XPS. All three methods gave corresponding results, a table of these results can be found in the appendix (Table A 1).

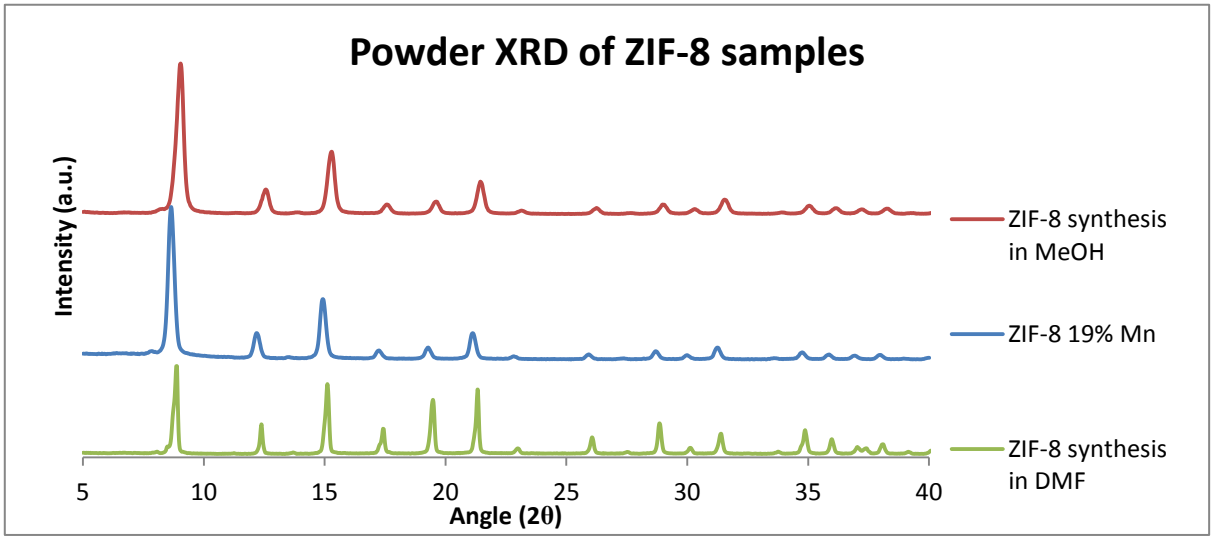

Figure 15. XRD patterns are shown of three different ZIF-8 structures; ZIF-8 synthesized in solvothermal conditions, in methanol at room temperature and after exchanging it with manganese.

The results on the ZIF-8 particles, exchanged with $Mn(acac)_2$ that were analyzed with AAS can be found in Figure 16. In this graph, the amount of samples prepared with a given percentage of manganese ions exchanged with zinc ions from the framework is plotted. All these samples were prepared by immersing ZIF-8 samples in a methanol solution containing 0.12 M $Mn(acac)_2$. The histogram makes it very clear that there is no real control over the amount of manganese exchanged by simply putting the ZIF-8 particles in solution at 55°C.

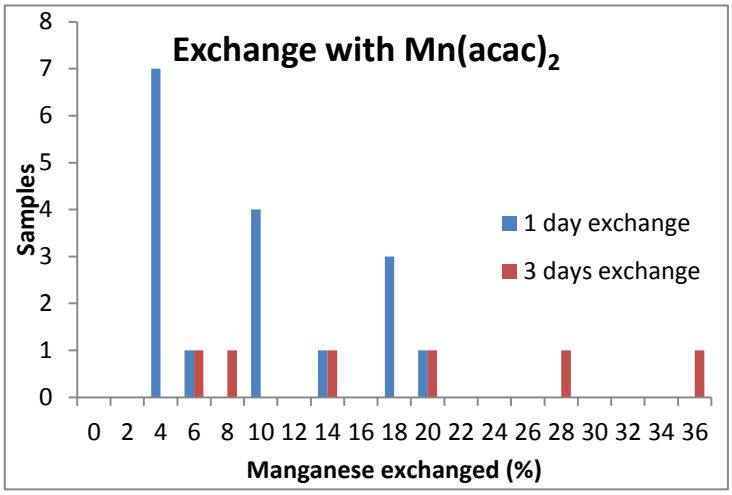

Figure 16. The percentage of zinc ions in the framework that are exchanged with manganese ions from the solution (x-axis) versus the amount of samples prepared (y-axis), measured with AAS. This histogram clearly shows that there is no control over the amount of manganese exchanged with the procedure described by Fei *et al.*[1]

It was assumed that longer exchange periods will result in higher exchange percentages, and so forth the duration was increased to 3 days. Although a few samples do show a higher percentage of manganese in the framework of up to 35%, two other samples only possessed 6 and 7%. By increasing the exchange time from 1 to 3 days, the total amount of manganese can increase by a large amount, but still there is a lack of control over the final amount.

2.4.2 Towards higher reproducibility

Since there was no control over the exchange rate with the method described by Fei *et al.,*[1] other possibilities were considered to get a higher control. First, the mechanistic effects were investigated; it was assumed that the variations in exchange rate can be explained by inconsistencies in the heating of the reaction mixtures in the oven. For this reason, a second method was applied where the reaction mixture was now heated in an oil bath. With this method, the mixture can now also be stirred by using a magnetic stirrer, leading to more homogeneously distributed manganese over the ZIF-8. Unfortunately, this method did not yield a higher control over the exchange rates. Two batches gave manganese percentages of roughly 9% while three other batches only contained 3 to 4%.

To solve the problems concerning the exchange rates, new methods were conceived. Three conditions were supposed to possibly have an effect on the exchange process; the acidity, the type of manganese(II) precursor and the solvent. Therefore, a set of experiments was performed with three different precursors: $Mn(acac)_2$, $MnCl_2.4H_2O$ and $Mn(NO_3)_2.4H_2O$ in methanol and water. It was tried to change the pH of the solvent to pH 7 or pH 10 by adding dissolved NaOH or diluted HCl. For all the mixtures this did not work out, because $Mn(OH)_2$ particles started to precipitate when the pH got higher than 7 for solvents containing nitrate and chloride complexes. For mixtures containing $Mn(acac)_2$ complexes, the pH was not brought to a lower pH than 8.7, since this complex acted as a buffer. As a result of the poor solubility of $Mn(acac)_2$ in water, this mixture was not used for the exchange process.

The results obtained with varying exchange conditions can be found in Table 2. It can be concluded from this table that none of the used methods resulted in reproducible exchange percentages. It seems that a higher pH in methanolic solutions containing $Mn(acac)_2$ results in higher exchange percentages, although more experiments have to be carried out to make a definite conclusion. Exchanging zinc ions in the framework with manganese from nitrate precursors resulted in a higher exchange rate than observed for acetylacetonate precursors.

	Manganese content (%)		
Complex	In methanol pH = 7*	Methanol pH > 7*	In water pH = 7
$Mn(acac)_2$	12.8 & 4.7	11.8 ± 5.2	-
$Mn(NO_3)_2.4H_2O$	9.3 & 31.8	24.5	FC
$MnCl_2.4H_2O$	FC	FC	FC

Table 2. Percentages of manganese in the framework (based on total amount of metal) measured with AAS. All exchange methods with $MnCl_2$ salts gave a framework collapse (FC) according to XRD measurements; exchange with nitrate complexes in water resulted in framework collapses as well. * $Mn(acac)_2$ methanolic solutions were brought to a pH of 8.7 and manganese hydroxide precipitates started to form in methanolic $Mn(NO_3)_2$ solutions for a pH higher than 7.2.

Exchange with the use of chloride complexes was an extremely fast process, within seconds of immersing the colorless ZIF-8 particles in solution, the particles turned slightly brown already. After incubation at 55°C for one hour, the particles were colored dark-brown and the solution was turning brown as well. This indicates that $Mn(mIm)_2$ complexes are dissolved in the solution. When using nitrate complexes in water, the same coloring of the solution was detected and XRD measurements showed a framework collapse as well. Furthermore, exchanging with $Mn(NO_3)_2$ in methanol resulted in a brown solution as well, but in contrast to the particles exchanged by using $MnCl_2$ these particles still resembled the XRD pattern of ZIF-8, although peaks decreased in size significantly.

For the AAS measurements, the ZIF-8 crystals need to be dissolved in water. For this purpose, the ZIF-8 is first dissolved in nitric acid and subsequently diluted in water. It was observed that brown particles of ZIF-8 exchanged with $Mn(NO_3)_2$ did not fully dissolve in nitric acid. This effect has also been observed for some batches of ZIF-8 exchanged with $Mn(acac)_2$. Although it is not fully clear what is the cause of this, it is thought that this increased stability to acid is actually an effect of present metal oxides or hydroxides. The particles dissolved easily after adding only a few drops of HCl.

2.4.3 Increase in metal concentration after exchange

After washing elaborately with methanol for three days it was expected that unbound Mn^{2+} species would all have been washed out of the pores and from the surface. The metal concentration in the sample, expressed in mmol/g ZIF-8, should not change after metal exchanging. However, when looking at the metal content in the framework (Table A 2, Table A 3 & Table A 4), it can be seen that the zinc content in the framework does not decrease (as much as the manganese content has increased), and sometimes even increases.

Although no leaching was observed in later catalytic experiments (Chapter 3), the first and easiest explanation for the increase in metal loading is that there are still many unbound or physisorbed metal ions or complexes on the surface. With FTIR it should be possible to prove that acetylacetonate species are still present in the particles. When inspecting the three spectra of $Mn(acac)_2$, ZIF-8 and ZIF-8[$Zn_{0.7}Mn_{0.3}$] in Figure 17, it can be seen that some of the characteristic peaks found for $Mn(acac)_2$ at 1018, 1255 and 1602 cm^{-1} – of which the band at 1602 cm^{-1} band is associated with the stretching of the carboxylates – are not found in the spectrum of ZIF-8[$Zn_{0.7}Mn_{0.3}$] in Figure 17. In the Raman spectra pictured in the appendix (Figure A 1), there was also no proof found that additional species were present.

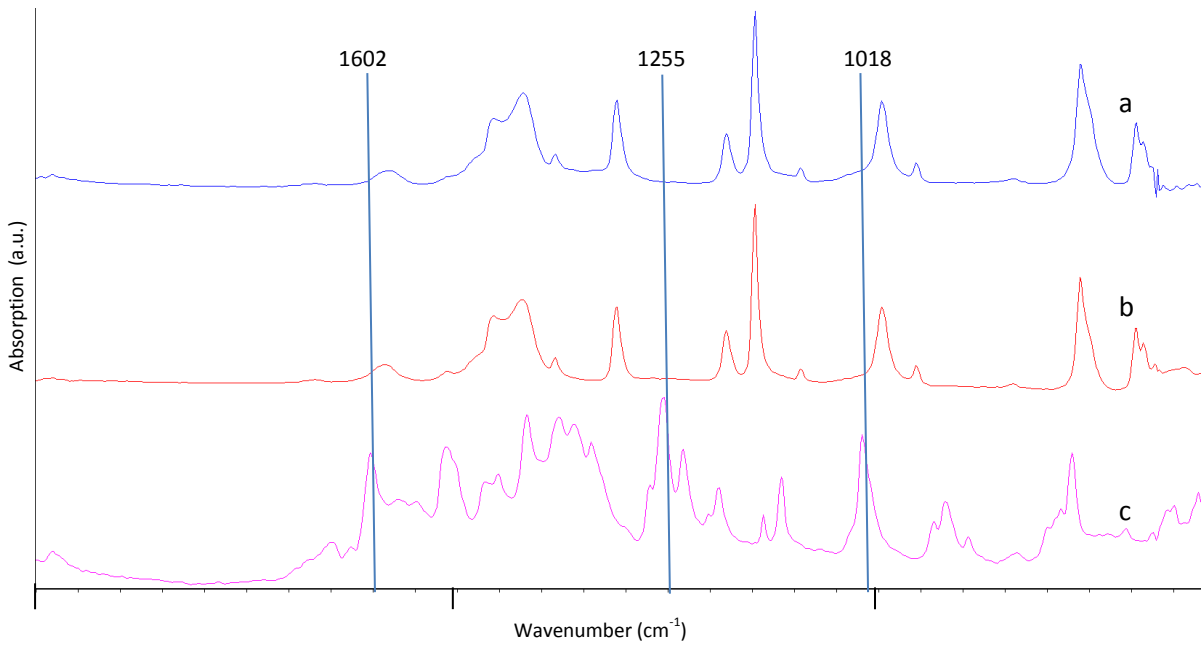

Figure 17. FTIR absorption spectra of ZIF-8 (a; blue), ZIF-8 [$Zn_{0.88}Mn_{0.12}$] (b; red) and $Mn(acac)_2$ (c; purple).

Additionally, evidence that multiples species are present in the particles is absent in the TGA curves (Figure 18). ZIF-8 [$Zn_{1-x}Mn_x$] does show lower stabilities as expected from the Irving-Williams series for metal imidazolate complexes,[80] but no information can be substracted from the figure that proofs the presence of additional species.

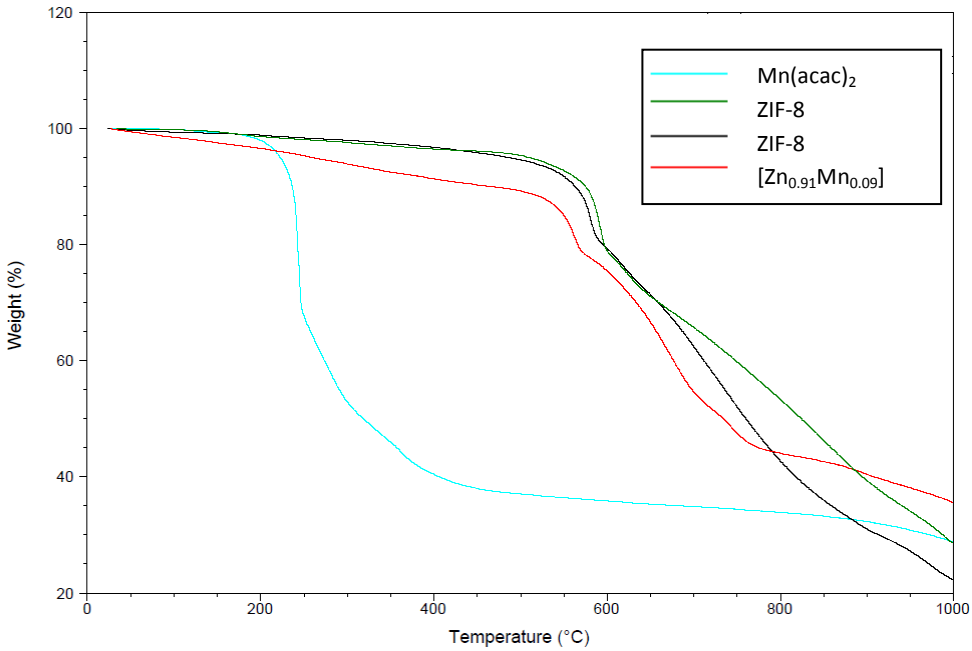

Figure 18. TGA curves for $Mn(acac)_2$, ZIF-8 plus two manganese exchanged species.

2.4.4 Framework disruption

XPS is a surface sensitive technique and measures the binding energies of electrons in the core shells of the elements. This binding energy (BE) is different for every element, but even more interesting is the fact that shifts in energies can also occur for the same elements in different environments, as explained in section 4.9. With this technique it should be possible to detect changes in environment for the elements by measuring changes in the BE for manganese and zinc 2p electrons and for nitrogen and oxygen 1s electrons.

For manganese and zinc, the BE for $2p_{3/2}$ seemed to be the same for every sample (between 1021.21 and 1021.37 eV for zinc and 640.92 and 641.11 eV for manganese), indicating that there is only one type of manganese and one type of zinc in the framework. Additionally, no shifts were observed for the binding energy of N 1 s for all the different samples. A shift was expected for different metal imidazolate complexes as a shift in binding energies also occurs in porphyrins prepared with varying metals.[81]

A striking result was observed in the XPS spectra for the O 1s binding energies. An increase in the atomic percentage of oxygen was detected in all the samples after the exchange process (Figure 19), suggesting that oxygen species are present at the surface of the framework after the exchange process. Besides a main peak at 530.8 eV, a shoulder in the O 1s peak with a binding energy of 528.5 eV was observed for all the manganese exchanged samples, but not for the original ZIF-8, implying that there were two different oxygen species present after exchanging.

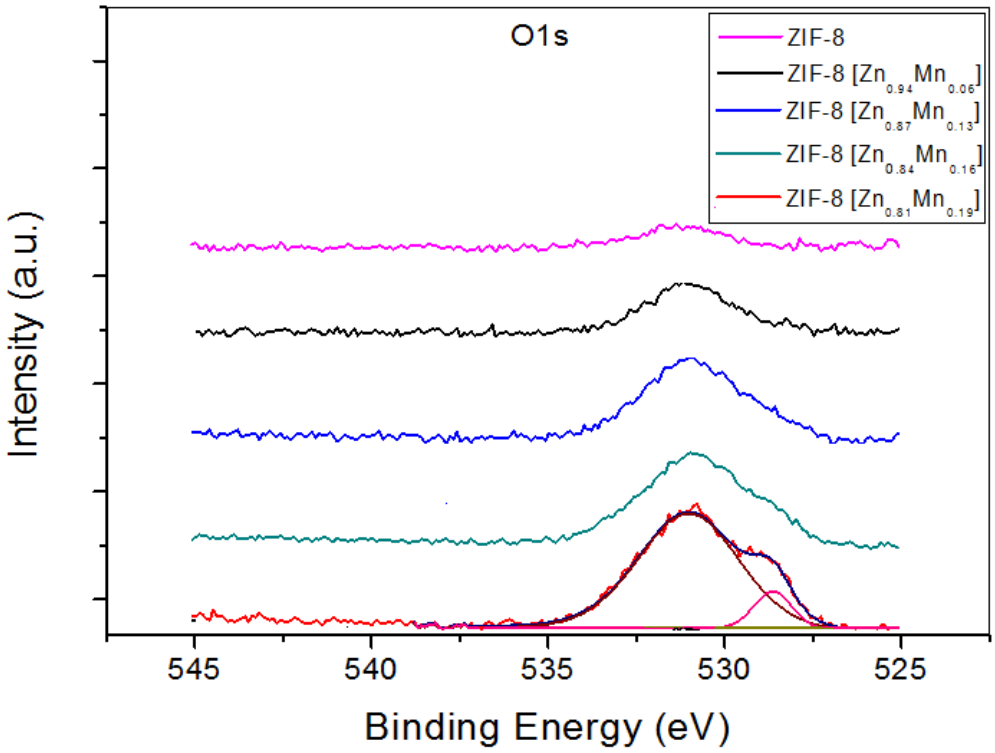

Figure 19. O 1 s binding energy of ZIF-8 particles containing different concentrations of manganese after exchanging for

The intense peak at around 530.8 eV can be assigned to metal hydroxides, $M(OH)_2$.[82] If these insoluble particles exist in the pores of the framework of the material, it can explain the increased content of metal and oxygen, but this should also result in a smaller surface area.

When comparing the surface area of three ZIF-8 batches with varying manganese content it is indeed found that the surface area and pore volume are decreasing upon increasing manganese content (Table 3). However, it cannot explain the large amount of oxygen in the surface of the sample; the oxygen content in ZIF-8 [$Zn_{0.81}Mn_{0.19}$] is almost 7 times higher than the total manganese content and 1.3 times higher than the total metal content. The increase in oxygen content can thus not be ascribed by the formation of $M(OH)_2$ alone. Oxygen molecules in adsorbed water and methanol molecules are expected to have a binding energy of approximately 534 eV and are therefore not expected to be present on the material, judging from the XPS spectra.[83] Also other possible candidates that could cause an increase in the oxygen content, such as CO_2 and O_2 have higher expected binding energies for O 1s. Furthermore, this could not explain why ZIF-8 itself has very little oxygen species present, as this sample has been in contact with air for the same amount of time. All weakly bound species are expected to have binding energies of higher than 531 eV.[82]

The most logical explanation would be that there is formation of zinc or metal hydroxides and that that manganese(II) ions are partially getting oxidized during the exchange process and maybe even during the washing step in technical grade methanol. This is in agreement with the peak at 531 eV, that is associated with $M(OH)_2$ and the shoulder at 528.5 eV that is most likely caused by Mn_2O_3 species.[84]

Table 3. Surface area and micropore volume of ZIF-8 before and after exchange determined by BET and t-plot methods.

Sample	BET Surface Area (m^2/g)	t-Plot Micropore Area (m^2/g)	t-Plot Micropore Volume (cm^3/g)
ZIF-8	1310	1234	0.62
ZIF-8 [$Zn_{0.9}Mn_{0.1}$]	1309.6	1110	0.54
ZIF-8 [$Zn_{0.65}Mn_{0.35}$]	1150	962	0.47

In Figure 20, the isotherms for ZIF-8 and its manganese exchanged variant ZIF-8 [$Zn_{0.75}Mn_{0.35}$] are depicted. Both isotherms clearly resemble the IUPAC isotherm Ia, as a result of their microporous structures. A few deviations in the isotherm for ZIF-8 [$Zn_{0.75}Mn_{0.35}$] are observed when comparing with ZIF-8. The first one is that the micropore volume per gram is smaller than that of ZIF-8, which is also seen in Table 3. A second observation is that absorption increases more from 0.1 to 0.8 P/P_0, which indicates that there are more macropores present. The third discrepancy can be found in the desorption isotherm of ZIF-8 [$Zn_{0.75}Mn_{0.35}$]; a hysteresis is observed, indicating that macro- and/or mesopores are present with narrow apertures.

All these observations lead to the conclusion that the structure of the framework is not fully retained after exchanging the zinc ions with manganese. It is hypothesized that the bonds at the small pores are destroyed during the exchange process, resulting in undefined supercages with small entrances. For 1 day exchange ZIF-8 with approximately 10% manganese, smaller pores and a larger increase in absorption from 0.1 to 0.8 P/P_0 were observed (indicating more mesopores), however no hysteresis was seen in the isotherm (Figure A 2 in the Appendix). It is thought that the breaking of smaller cages will take place after a certain amount of manganese is introduced to the crystals; the strain for the crystal becomes too high as manganese-imidazolate complexes are less stable and prefer octahedral geometries.

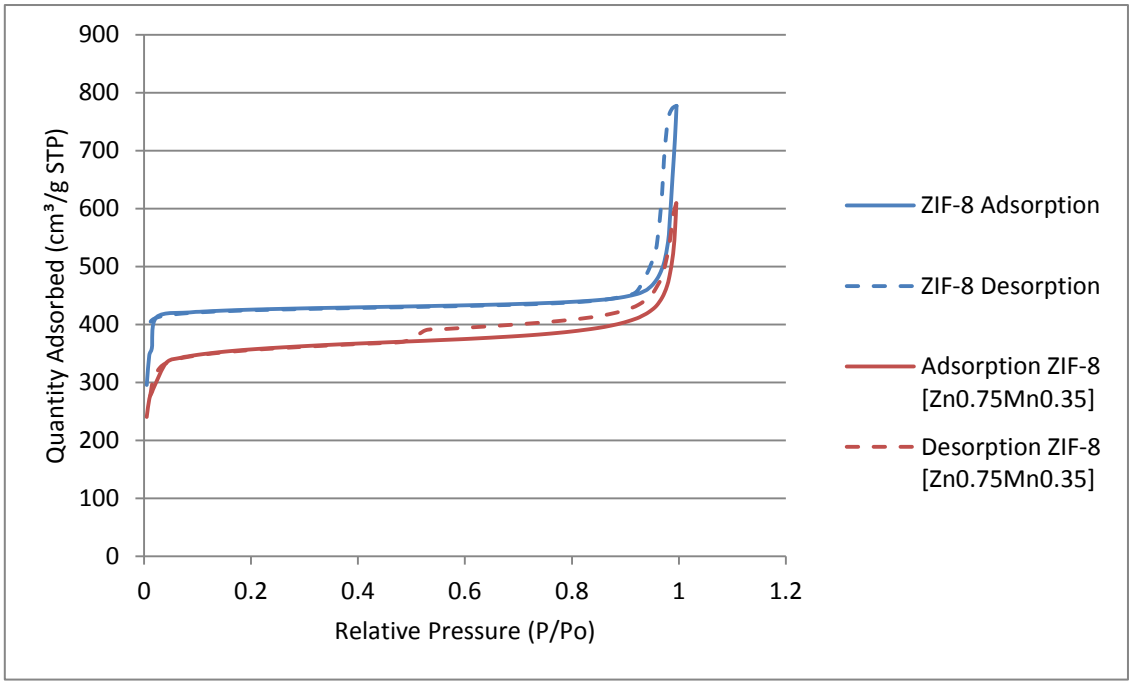

Figure 20. N_2 physisorption isotherms of ZIF-8 and ZIF-8 [$Zn_{0.75}Mn_{0.35}$] prepared by immersing the ZIF-8 in methanolic $Mn(acac)_2$ solution for 3 days at 55 °C.

2.5 Conclusions

It was attempted to reproduce the method by Fei *et al.*[1] to synthesize ZIF-8 crystals with manganese ions in the framework. By immersing the particles in a methanolic $Mn(acac)_2$ solution for 1 day, exchange yields of 2 to 20 % were obtained. By increasing the exchange period to 3 days, this yield could be increased to 35%. The washing and drying steps were proven to be successful as there were no additional $Mn(acac)_2$ species seen with the use of TGA, FT-IR and Raman spectroscopy. However, since the zinc content did not decrease (as much as the manganese content has increased), it was thought that introduced manganese ions are not fully incorporated into the framework.

Changing the combination of solvent, pH and manganese precursors did not improve results. Water was found not to be an appropriate solvent since it resulted in a framework collapse. Exchange with $MnCl_2$ was a very fast process and resulted in a framework collapse in water and methanol as well. $Mn(NO_3)_2$ did result in a higher exchange rate, but also in a lower crystallinity.

In the XRD patterns, a shift to lower 2θ is expected when a metal is introduced with a larger ionic radius. However, no shift was observed in the XRD patterns, only a decrease in peak height and an increase in noise were measured. Both of these results indicate that the amount of manganese introduced to the framework is either very low or random. In addition to the XRD results, a decrease in surface area and pore volume is detected with increasing manganese content in the physisorption results, while a small increase is expected for ZIF-8 with manganese. This is most likely caused by the formation of $Mn(OH)_2$ and Mn_2O_3 species, observed with XPS. Above all, no zinc was detected with AAS in the solutions after the exchange process, indicating that the zinc had not left the framework.

These results do not fully proof that manganese has not been exchanged at all. However, they do indicate that besides exchanging the metals, other processes are taking place.

2.6 Outlook

Since the results indicate that the exchange methods with manganese were not reproducible and there was not an unlimited amount of time; some ideas have come up which could lead to a better understanding of the exchange process that have not been worked out. These ideas are presented in this subchapter.

2.6.1 Alter the exchange conditions

An increase in the amount of oxygen species was detected with XPS after exchange had taken place with $Mn(acac)_2$, an explanation is that manganese gets oxidized during the exchange process by oxygen or water present in the technical grade methanol. By using inert conditions and absolute methanol during the exchange of zinc with manganese this should not be possible and this problem could be solved.

Another problem is that manganese, coordinated to imidazolates, prefers low-spin octahedral geometries. It is hypothesized that by a fast exchange process and high exchange yields, the strain will get too high for the framework and the framework will get disrupted. By using different manganese precursors and concentrations, this can be optimized to yield ZIF-8 structures consisting of zinc and manganese ions, without losing its original structure. Manganese oxalate for instance, has a tetrahedral geometry and could force the manganese to stay in this geometry.

2.6.2 Exchange with other metals

Although manganese is a very interesting metal for catalysis, this metal has a lower stability in complexes than zinc. Other interesting candidates for performing PScE are nickel and copper since their stability is higher than that of zinc. As the direct synthesis of ZIF-8 with cobalt (ZIF-67) is already possible, this is a less interesting candidate but could be used for the proof of concept. Also, exchange with zinc(acac)$_2$ is an interesting experiment to measure if any changes occur during the synthesis. Since cobalt, nickel and copper have more attractive spectroscopic properties in the UV-vis region than both zinc and manganese, these properties can be gained to get more insight in the process.

2.6.3 Characterization Techniques

With other characterization techniques more insight in the obtained structure can be obtained. For instance, with X-ray Absorption Fine Structure, the local structures and electronic states of the elements can be determined and with (solid state) ^{1}H-NMR, changes in the environment of the protons in the imidazole ring can be detected. These methods could give a clue to where the metal elements are located and if they are bound to the imidazolates.

Chapter 3

CATALYTIC TESTING OF ZIF-8 [$Zn_{1-x}Mn_x$]

3.1 Introduction

As a result of the fact that ZIF-8 crystals are composed of Zn^{2+} ions connected by 2-methylimidazolate linkers, it is expected that it has a low catalytic activity in oxidation reactions. Zinc(II) does not have free space in the d-orbitals that can be used in catalytic activity since it has a fully filled d^{10} orbital. Manganese on the other hand can change oxidation state relatively easy and is able to form weaker covalent bonds between ligands. This makes PScE of ZIF-8 by exchanging the zinc ions with manganese an interesting candidate for additional catalytic properties as its thermal and chemical stability is rather high in comparison with alternative MOFs. Manganese based MOFs have been prepared and were found to be an effective catalyst in multiple studies on the epoxidation of olefins.[66,85,86]

ZIF-8 has been used in multiple studies for the sieving of molecules and this can also be applied for catalysis. Owing to its extremely high surface area as a result of the well-defined pores, a difference in reaction rate is expected for substrates that fit into the pores and substrates that will not. ZIF-8 has a pore aperture of 3.4 Å, but is able to adsorb and sieve molecules of up to 6.3 Å as a result of its flexible structure.[87] This means that many unbranched olefins and even cyclohexene will be able to enter the framework, in contrast to larger molecules such as cyclooctene[88] (Figure 21). A higher conversion is predicted for 1-hexene and cyclohexene in comparison with cyclooctene as they are able to enter the pores whereas cyclooctene is not.

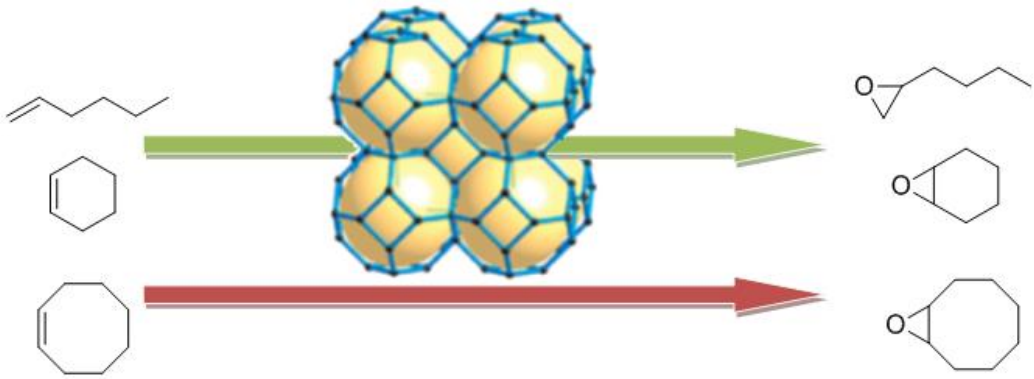

Figure 21. Epoxidation of different olefins, varying in size. As a result of their size, 1-hexene and cyclohexene are able to pass through the pores, while cyclooctene is only able to react on the outer surface.[87] The ZIF-8 structure is taken from reference [13].

The valorization of biomass is becoming more and more important as the oil prices are increasing. Lignin, as one of the most abundant organic polymers found on earth, can play an important role in the search for renewable resources. By depolymerization of lignins and oxidizing the monomers with the use of catalysts, new functional aromatic compounds can be synthesized.[89] Veratryl alcohol is a substructure that can be found in lignin and was used for the testing of manganese exchanged ZIF-8 (Figure 22). In an earlier study, the cobalt based ZIF-9 was used as a heterogeneous catalyst for the oxidation of this (and other) substrates and it was found to be a good alternative for homogeneous catalysts.[90] Although no leaching of the metals was found in this work, the framework was altered over the long range. With the higher stability of ZIF-8 and the more environmental friendly manganese, this new catalyst could be a promising candidate. As the pores of ZIF-8 with a maximal

aperture of 6.3 Å are too small for the substrate to enter, only reactions will take place at the outer surface of the particles. For a higher activity, a manganese exchanged version of ZIF-70 [Zn(Imidazole)$_{1.13}$(nitroimidazole)$_{0.87}$] with a pore aperture of 13.1 Å could be used.

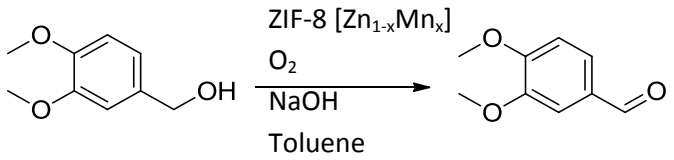

Figure 22. Catalytic oxidation of veratryl alcohol to veratraldehyde.

In this chapter, exchanged ZIF-8 [$Zn_{1-x}Mn_x$] crystals are used as a catalyst in the previously described reactions, namely, the oxidation of veratryl alcohol to veratraldehyde and the epoxidation of 1-hexene and 1-octene to respectively 1-epoxyhexane and 1-epoxyoctene.

3.2 Methods

3.2.1 Materials

The following materials were used as received:

- ZIF-8, as synthesized in section 2.3.2
- ZIF-8 [$Zn_{1-x}Mn_x$], as synthesized in section 2.3.2
- Sodium hydroxide [NaOH, Merck, 99%]
- Methanol [MeOH, Interchema, Pract.]
- Dichloromethane [DCM, Interchema, Amylene stabilized]
- Acetonitrile [ACN, Acros 99.8%]
- Anisole [$CH_3OC_6H_5$, Acros, 99%]
- Veratryl alcohol [$C_9H_{12}O_3$, Sigma-Aldrich, 96%]
- 1-hexene [C_6H_{12}, Acros, 97%]
- 1-octene [C_8H_{16}, Acros, >99%]
- Hydrogen peroxide [H_2O_2, Merck, 30% w/v aqueous solution]
- Hydrogen peroxide [H_2O_2, Sigma-Aldrich, 50% w/v aqueos solution]

3.2.2 Oxidation of Veratryl Alcohol

39 mg of ZIF-8 or exchanged derivatives, 40 mg NaOH, 5.0 g toluene and 0.68 g veratryl alcohol were weighed and mixed in a steel autoclave. The autoclave was purged with oxygen and a final pressure of 5 bar oxygen was applied. The autoclave was subsequently heated to 150 °C under vigorous stirring of 1000 rpm. After a reaction time of 4 hours, the autoclave was cooled by using an ice bath. The particles and solution were separated with a pipette and the solution was filtered afterwards. The solution was then stored in the fridge.

To measure the conversion of veratryl alcohol to veratraldehyde, 0.6 mL sample was mixed with 7.5 mL ethanol to which 0.8 mL internal standard was added. The internal standard was prepared by adding 3 g anisole to 10 g toluene.

3.2.3 Peroxidation of Olefins

10 mg of dry ZIF-8 [$Zn_{0.82}Mn_{0.18}$] (equivalent of 8.5 µM manganese) was weighed and added to 2.5 or 5.0 mL methanol in a 20 mL round-bottom flask while stirring. 0.57 mL 30% w/v (5 mmol) or 0.68 mL (10 mmol) 50% w/v aqueous solutions of H_2O_2 were slowly added. The mixture was subsequently heated or cooled to the desired temperature of 0, 20, 40, 60 or 80 °C; 0.63 mL (5 mmol) 1-Hexene or 0.79 mL (5 mmol) 1-octene was added to the mixture after reaching the desired temperature. After 4 hours, the reaction was stopped by immersing the flask in an ice bath followed by a separation of the particles and the solution with a pipette. The solution was stored in the fridge.

A qualitative measurement was performed to detect any remaining H_2O_2 with starch paper; GC was used to measure the conversion of the olefins to epoxides by adding 0.5 mL to 1 mL methanol.

3.3 Results and discussion

3.3.1 Epoxidation of olefins

No additional species were detected in the GC spectrum, apart from the 1-hexene or 1-octene peaks at respectively 2 and 4.5 minutes. The chromatograms are depicted in Figure A 3 and Figure A 4 in the Appendix.

In addition to the GC results, a qualitative measurement with starch paper was performed on the solution to detect any remaining H_2O_2. In all experiments, with varying temperatures (20, 40, 60 and 80 °C), solvents (methanol or acetonitrile) and H_2O_2 to substrate ratio (1:1 and 2:1), the starch paper did not change color, indicating that although no epoxidation of the substrate has taken place, the peroxide had been reduced. No experiments have been carried out to find out what has been oxidized by the peroxide, it is however possible that manganese(II) is oxidized to manganese(III) during the reaction, as the color of the particles changed from pale brown to a more darker brown color. Another explanation for the decomposition of H_2O_2 is that a Fenton's type reaction is taking place, which leads to unselective oxidations.

3.3.2 Oxidation of veratryl alcohol

For the oxidation of veratryl alcohol, ZIF-8 with variable manganese loading were used and compared. Initially, the results appeared to be very promising. A conversion of 10% for ZIF-8 and an increase to 71% after exchanging with manganese to ZIF-8 [$Zn_{0.7}Mn_{0.3}$] was found. For an experiment with $Mn(acac)_2$ as catalyst, the same molar ratio of manganese to substrate was used, and also a similar conversion was found of 72%.

To determine if leaching of homogeneous metal species from the catalyst was taking place, a hot filtration experiment was performed with ZIF-8 [$Zn_{0.81}Mn_{0.19}$]. After 1 hour, the catalyst was filtered from the reaction mixture and the reaction continued in a clean autoclave for 3 more hours. After 1 hour, the conversion was 47% already and no increase in the conversion was found after the solid particles were filtered off. For this experiment, the solution after the hot filtration was measured with ICP-OES for any manganese species in the solution. A concentration of $40 \cdot 10^{-3}$ $\mu mol \cdot L^{-1}$ Mn was found in the solution, indicating that only $6 \cdot 10^{-3}$ % of the manganese from ZIF-8 [$Zn_{0.7}Mn_{0.3}$] was leached. Dissolved zinc ions were measured as well and it was found that $6 \cdot 10^{-2}$ % zinc was leached from the catalyst. These quantities were so small that they were out of the calibration range and might as well be an effect of noise.

Further experiments gave inconsistent results. As the blank conversions went up to more than 20%, it was thought that the reaction of veratryl alcohol to veratraldehyde was also catalyzed by contaminents in the autoclave. All the results of the oxidation reactions can be found in Table A 5 in the Appendix.

All the blanks had solid depositions after the reaction and these were measured with AAS and analyzed with an element scan. The metals detected that had a significant absorption were: Cu, Fe, Mg, Mn, Mo, Na, Ni and Zn (Table 4). It is not known in what kind of state these elements are present during the reaction, however, it is speculated that these elements can act as a catalyst as well, partially dissolved or as a heterogeneous metal oxide/hydroxide.

Table 4. Element scan with AAS of the solids precipitated after a reaction without adding catalyst (blank reaction). The solids were dissolved in an aqueous solution with nitric acid.

Element(λ)	Cu(324)	Fe(248)	Mg(285)	Mn(279)	Mo(313)	Na(588)	Ni(232)	Zn(213)
Absorption	0.00031	0.00891	0.00061	0.00074	0.00074	1.2142	0.00339	0.00126

3.3.3 The catalyst after the reaction

After the (manganese exchanged) ZIF-8 crystals were used as a catalyst, infrared measurements were performed to detect impurities present on the particles (Figure 23). The IR spectra make clear that after washing, many impurities are still present at the catalyst, as indicated by the strong water or alcohol bands at wavelengths above 3000 cm^{-1}. Many peaks have disappeared after immersing the particles in dichloromethane for a day, however there are still some impurities present. Additionally, an intense peak at 1639 cm^{-1} is observed, which is associated with the C=O stretch of veratraldehyde or with an amide. The C=O stretch in veratraldehyde is expected to have a sharp absorption peak at 1670 cm^{-1} or higher.[50] Therefore, it is more likely to be an amide. The presence of an amide is unexpected and the origin is not known exactly. A possible explanation could be that (weakly coordinated) 2-methylimidazoles are getting oxidized during the reaction to 2-methylimidazolones which has been observed in earlier performed homogeneous reactions.[91] If this is occurring only for weakly bound imidazoles at defects or at the surface, or if this happens over the whole structure is not known. An assignment of a selection of the peaks can be found in the Appendix in Table A 6.

After the oxidation reaction, the crystallinity is retained, however, the intensity of the peaks at low 2θ angles is greatly reduced, indicating that the average crystallinity of the structure is somewhat reduced (Figure 24).

Due to time limitations, no reactions were performed with recycled catalysts.

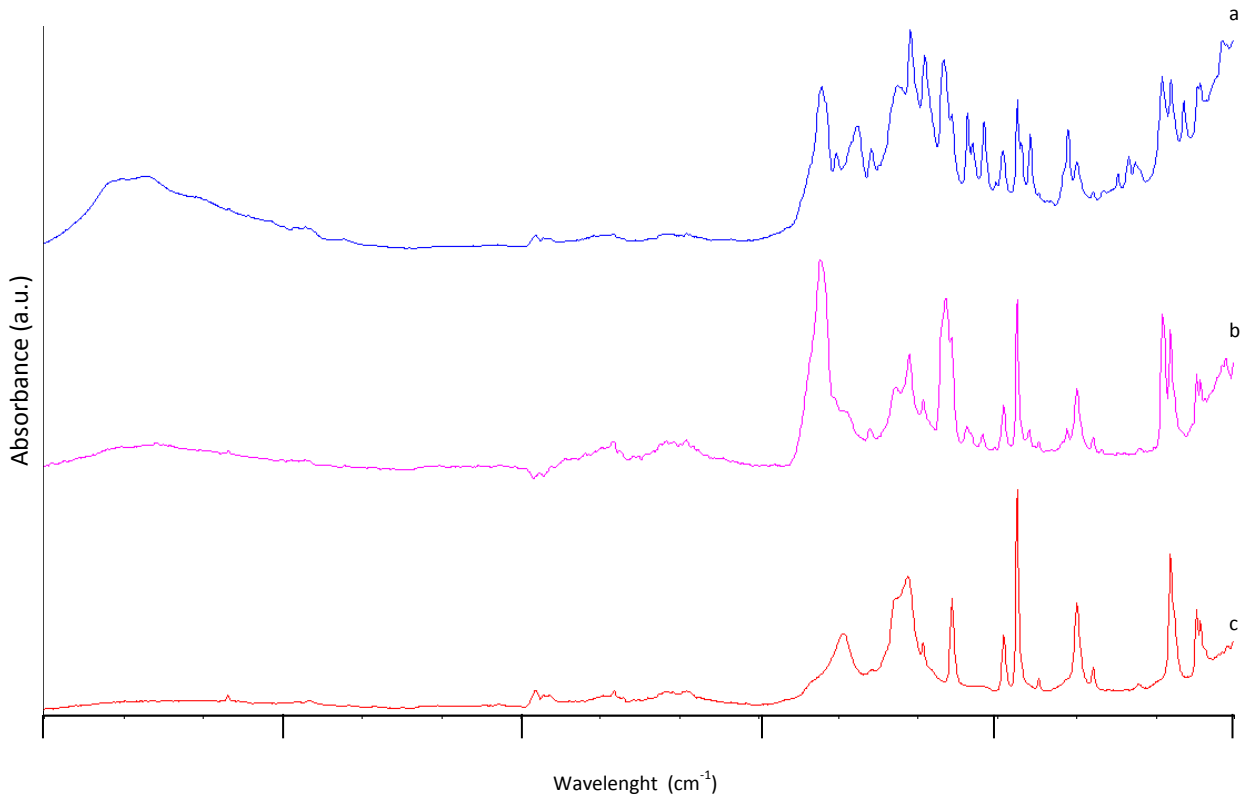

Figure 23. IR spectra of ZIF-8 [$Zn_{0.7}Mn_{0.3}$] after the oxidation reaction of veratryl alcohol to veratraldehyde and a subsequent washing step with toluene (a; blue), after immersing for a day in dichloromethane (b; pink) and as-synthesized (c; red).

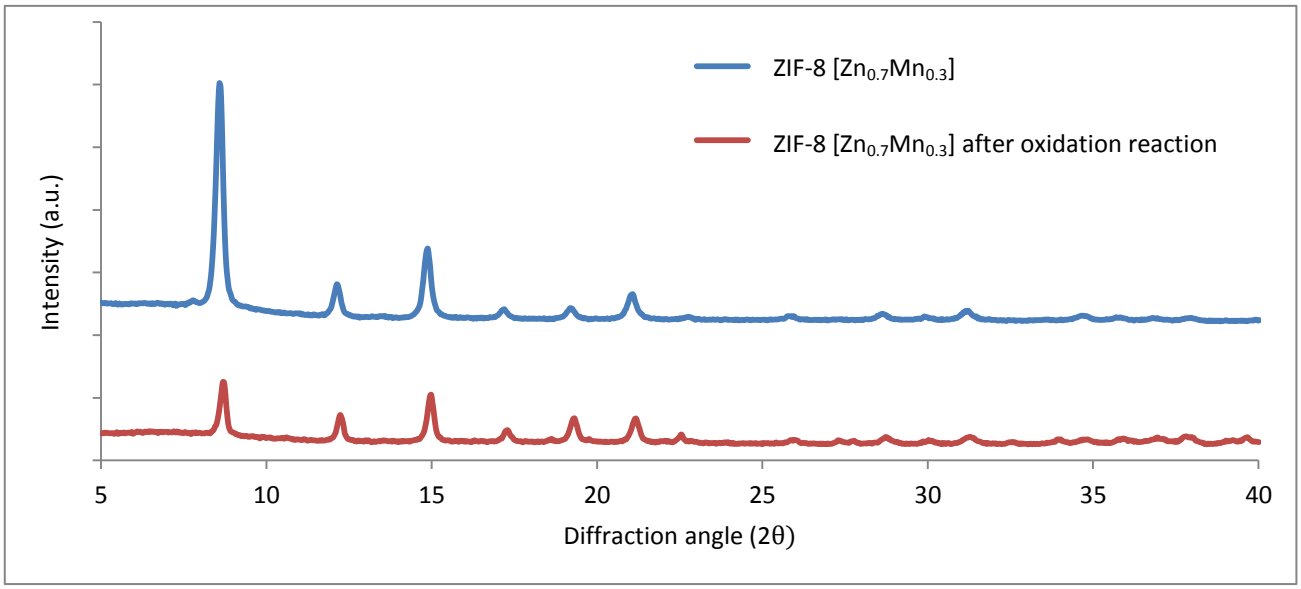

Figure 24. XRD patterns of ZIF-8 before (above; blue) and after (below; red)

3.4 Conclusions

Inconsistent results were obtained for the catalytic testing. Although it is evident that by adding ZIF-8 [$Zn_{1-x}Mn_x$], the activity is increased for the oxidation of veratryl alcohol to veratraldehyde, it is not known what its precise influence is on the reaction. This is caused by contaminants in the autoclave, which probably originate from the autoclave itself or from previously performed reactions.

ZIF-8 does not leach manganese or zinc ions during the reaction and remains a solid. Small differences are observed in the XRD pattern, which indicate that the crystal structure is retained, but that the average crystallinity of the total structure has decreased. After washing with toluene and immersing them in dichloromethane, the particles still exhibit some additional bands in the IR spectra, indicating that there are still some additional organic molecules present in the pores or at the surface. Additionally, an intense peak at 1639 cm^{-1} was observed which is possibly the result of an oxidation reaction of 2-methylimidazole to 2-methylimidazolone.

Manganese exchanged ZIF-8 did not show any catalytic activity for the reaction of 1-hexene or 1-octene to their respective epoxides. With GC, no molecules have been detected other than the solvent used and the substrates. It is hypothesized that hydrogen peroxide is consumed during the reaction to oxidize manganese in the ZIF-8 crystals without the manganese being capable of subsequently oxidizing the olefins.

3.5 Outlook

A future plan to increase reproducibility over the oxidation reactions of veratryl alcohol would be to use a clean autoclave to measure the activity of the catalysts. As the conditions used in the experiments are not extremely demanding, the experiments can also be performed in a glass round-bottom flask. It will be less complicated to clean the flask of any contaminating metals with acids, and instead of using a higher pressure system, oxygen can be bubble through the solvent and a cooler has to be added to reflux toluene.

Since oxidation with ZIF-8 [$Zn_{1-x}Mn_x$] was successful with oxygen present, this method can also be used for the epoxidation of olefins or oxidation of small unbranched molecules. This can then be used to compare the catalytic activity for molecules that fit into the pores and for those that do not.

Reactions with recycled catalysts have not been carried out yet, and should be performed. Additionally, experiments with milder conditions should be performed so that the catalyst will have a higher chance of surviving the reactions.

Chapter 4

CHARACTERIZATION TECHNIQUES

4.1 Infrared and Raman Spectroscopy

Infrared (IR) and Raman spectroscopy are both non-destructive vibrational spectroscopic techniques. Both techniques measure vibrational energy levels that are associated with the chemical bonds in the sample. Since spectra are unique for every molecule, it can be used for the characterization of materials. IR and Raman spectroscopy both work on different principles, which are explained in this section.

Fourier Transform Infrared Spectroscopy (FTIR) is a very easy and therefore widely used method to carry out qualitative measurements. The mid-IR region covers the region from 25 to 2.5 µm (400 to 4000 cm^{-1}) and in this region most matter will absorb light very specifically, depending on the elements and functional groups present.

Infrared light interacts with matter by increasing the energy from a state E_i to E_f and the energy difference between these two states is absorbed only if the frequency *v* is:

$$v = \frac{E_f - E_i}{h}$$

As the energy of light in the mid-IR region corresponds to the energy differences for rotations and vibrations within molecules, it is capable of exciting it to higher rotational and vibrational levels. Vibrational transitions are much higher in energy than rotational transitions and will be observed at higher frequencies. Stronger bonds and bonds between atoms with a lower reduced mass will have higher vibrational frequencies and the corresponding energies are therefore higher as well. Only vibrational transitions are allowed that will cause a change in the dipole moment are allowed and detected with IR spectroscopy. Other absorptions in this region are detected with Raman spectroscopy.[92]

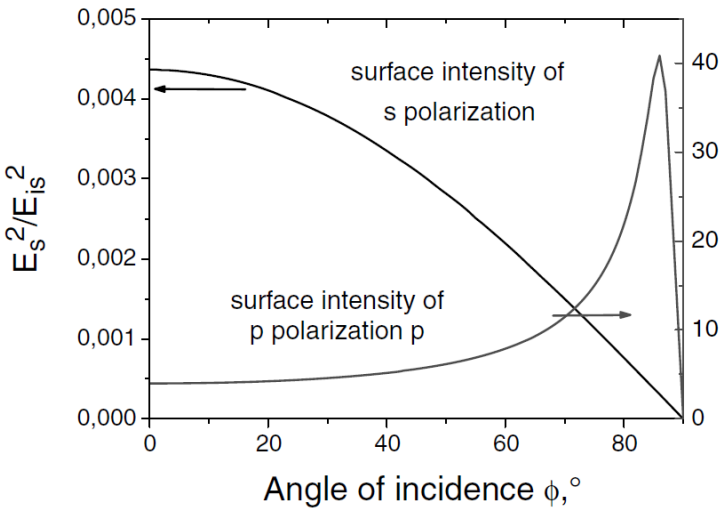

Figure 25. A change in light intensity for s- and p-polarized light is observed in the vicinity of the surface as a result of a varying angle of incidence.[93]

Grazing angle IR works with the fact that p-polarized light has constructive interference when reflected at the surface with a grazing incident angle, while s-polarized light has destructive interference. This is a result of a phase shift occurring for both p- and s-polarized light. For s-polarized light, the phase shift will be 180° upon reflectance, no matter what incident angle is used (Figure 25 &Figure 26). This is in contrast to p-polarized light, where the phase shift is dependent on the angle of incidence. The sensitivity for molecules at the surface will be greatly increased for p-polarized light as a result. Together with an inert environment and a p-polarizer, the sensitivity for adsorbed molecules will be even greater.[93]

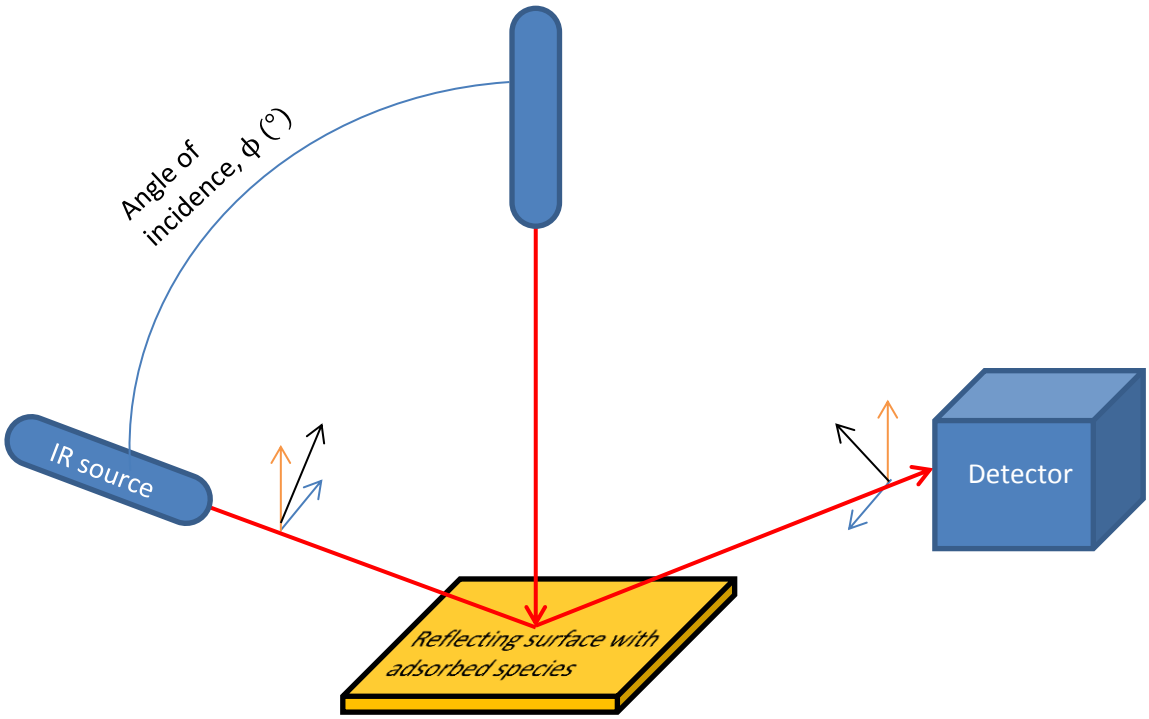

Figure 26. Basic principles of grazing angle IR. The phase shift of p- and s- polarized light can be observed in the image as well. For s-polarized light (E_{is}), the phase shift will be always 180° upon reflection (E_{rs}). The phase shift for p-polarized light is dependent on the angle of incidence.

Whereas IR spectroscopy originates from the fact that absorption of photons takes place when a vibrational level in the ground state gets excited, Raman spectra have their origin in the electronic polarization of material caused by UV, visible or near-IR light. If monochromatic light with a frequency *v* irradiates a molecule, the light will get scattered as a result of the electronic polarization induced in the molecule by the light. The scattered light will have frequency *v* (Rayleigh scattering) or $v \pm v_i$ (Raman scattering), where v_i represents a vibrational frequency of the molecule.

Although Raman scattering is more than 1000 times lower in intensity than Rayleigh scattering, it is still possible to detect it by using a strong excitation source, for example a laser. Raman scattering is much more interesting than Rayleigh scattering, as this will give complementary information on the composition of the molecule with respect to IR spectroscopy; dipole forbidden transitions are observed with Raman spectroscopy.[94]

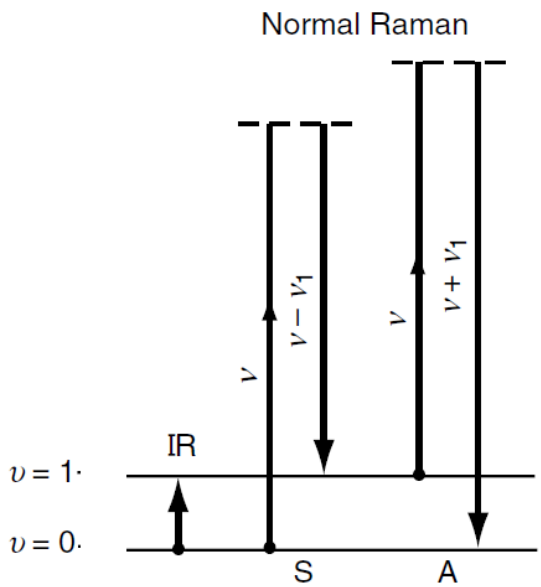

Figure 27. Mechanisms of IR and normal Raman, S and A denote stokes and anti-stokes scattering. This figure is an adapted image taken from reference [94].

Owing to the fact that IR and Raman spectroscopy are such widely used methods, many materials have been studied already and expected absorption

energies for a large group of elements and functional groups have been published in books giving an overview, for instance the one written by George Socrates.[50] This book has been used for the characterization of the materials prepared during this research.

ATR-IR Instrumentation

Infrared spectroscopy measurements were carried out at room temperature on a Bruker Tensor-27 or Tensor-37 IR spectrometer equipped with a Pike MIRacle ATR accessory. 16 to 32 scans with a resolution of 4 cm^{-1} over a range of 600 – 4000 cm^{-1} were taken of each sample.

Grazing Angle IR Instrumentation

Grazing angle IR is performed on a Perkin Elmer system 2000 FT-IR, equipped with a Monolayer/Graseby Specac Grazing Angle Specular Reflactance Accessory and an MCT detector. 1000 scans with a resolution of 4 cm^{-1} over a range of 600-4000 cm^{-1} were taken of each sample. Incident angles varied between 75° and 86°.

Raman Spectroscopy Instrumentation

All Raman spectroscopy measurements were carried out at room temperature with a Renishaw Invia Raman microscope. Raman spectra were measured with a 1200 $l \cdot mm^{-1}$ grating and a ½ inch RenCam CCD detector over a range of 100-3500 cm^{-1}. For measurements of bulk products, a 785 nm red laser was used and for SURZIFs, a 532 nm green laser was used.

4.2 Gas Chromatography

Chromatography is essentially a separation method in which components are distributed over two phases: the stationary phase and the mobile phase. The process occurs as a result of repeated sorption and desorption of the components along the stationary bed. The separation takes place as a result of different distribution constants of the individual components within the solvent. In gas chromatography the mobile phase is an inert gas, which is led through a tube covered with an inert stationary phase, such as methyl polysiloxane.

In gas chromatography, the difference in retention time is caused by different boiling temperatures of the components. The concentration of the components can be determined by a flame-ionization detector. Carbon containing components will form cations and electrons upon pyrolysis, which generates a current between the electrodes. This increase in current is translated to a signal increase in the chromatogram.[95]

Instrumentation

Gas chromatography is performed on a Varian 430-GC with an Agilent Technologies VF-5MS column (30m/0.25mm/0.25µm). To measure the oxidation of veratryl alcohol, the sample was injected at 40 °C and heated with a ramp of 20 $°C \cdot min^{-1}$ to 120 °C at which it was kept for 5 minutes. It was then heated to a final temperature of 180 °C with a ramp of 20 $°C \cdot min^{-1}$ and this was maintained for 20 minutes. For the measurement of the oxidation reaction of olefins, the sample was injected at 40 °C and heated with a ramp of 10 $°C \cdot min^{-1}$ to a final temperature of 200 °C.

The sample was prepared as follows: 0.6 mL sample was mixed with 7.5 mL ethanol, to which 0.8 mL internal standard was added. The internal standard was prepared by adding 3 g anisole to 10 g toluene. Calibration solutions were prepared in the same manner.

4.3 X-Ray Diffraction

When X-rays hit a sample, the waves will scatter and produce a pattern of stronger and weaker sum-waves; known as a diffraction pattern. The direction of diffracted beams is determined by the geometry of the sample alone, and not by the position of individual atoms in the unit cells. Therefore this technique can be used to measure the crystalline structure of materials.

X-ray photons can either travel in a straight line through the lattice plain or be reflected by a plane under the same angle as the angle of incident. After elastic scattering takes place in the sample, two things can happen: constructive and destructive interference of the X-rays. Whether constructive or destructive interference takes place depends on the lattice spacing d_{hkl}, the wavelength λ and the diffraction angle θ. Only a signal will be detected when constructive interference of the X-rays occurs and this can be calculated with the Bragg equation:

$$2d_{hkl}\sin\theta = n\lambda$$

As a result of multiple d_{hkl} values, a pattern is observed when the sample is irradiated with a monochromatic X-ray beam and the intensity of the detected X-rays are plotted against the change in diffraction angle. For samples with dissimilar lattice spacings and/or other structures, different patterns are observed. This makes XRD a strong method to determine the crystalline structure.[96]

Instrumentation

Room temperature XRD measurements are carried out on a Bruker-AXS D8 Advance powder X-ray diffractometer, in Bragg-Brentano mode, equipped with automatic divergence slit and a PSD Våntec-1 detector. The radiation used is Cobalt Kα1,2, λ = 1.79026 Å, operated at 30kV, 45 mA. prim. Soller slit 2,5° automatic divergence slit: 0.6 mm 0.3° antiscatter slit 2.44 mm det. slit 3.54 mm PSD angle: 1° θ –θ system 435 mm radius. Most of the measurements were performed in the region 2θ = 5-40°, since many characteristic peaks for ZIFs can be found in this range.

4.4 Contact Angle Measurements

Contact angle measurements are based on a very easy principle. A small droplet of a pure liquid with a known and fixed volume is put on a substrate, after which the contact angle of the droplet with the substrate is measured. Differences in angles can be observed for changes in interactions between water and the surface of the substrate. For hydrophobic surfaces, the water will try to minimize contact with the surface and this will result in a large contact angle. This is in contrast to hydrophilic surfaces, where complete wetting or a very small angle is expected.

With contact angle measurements a qualitative result can be obtained to what functional groups are present at the surface and the homogeneity of the coverage after immersing a gold coated substrate in a solution with thiols.

Instrumentation
Contact angle measurements were performed with the Optical Contact Angle OCA15, with single dosing units. A USB-Wide-VGA camera was used, with a resolution of 752 x 480 pixels. The contact angles were calculated with the supplied software: SCA 20.

4.5 Thermogravimetric Analysis

With thermogravimetric analysis (TGA), the thermal stability of the sample can be determined as well as any additional species on the surface or in the pores. Under $N_{2(g)}$ flow, the temperature is increased steadily while the mass of the specimen is accurately measured. When a component evaporates, it is detected as a mass loss. A steep decrease in mass is detected when the sample decomposes at elevated temperatures.

Instrumentation
Thermogravimetric analyses were performed on a TGA Q50 instrument. 10 to 20 mg powder was weighed and put on a platinum pan. It was then heated under a nitrogen flow of 60 mL/minute to 1000 °C with a ramp of 5 °C/min.

4.6 N_2 Physisorption

Physisorption forces are the same forces that cause the condensation of gases and deviations from ideal gas behavior. It is thus a general process that occurs without much specificity. In contrast to chemisorption, molecules keep their identity without needing any activation energy to bind to the surface. In a N_2 physisorption experiment, nitrogen gas is slowly added to the sample at a temperature of 77K. As a result of van der Waals interactions, the molecules will condensate on the material and this results in a change in pressure.

With N_2 physisorption, an adsorption isotherm is measured and presented in a graphical form. From the shape of the isotherm alone, preliminary information can be obtained already, since the shape depends heavily on the type of material and its porosity (Figure 28).[97]

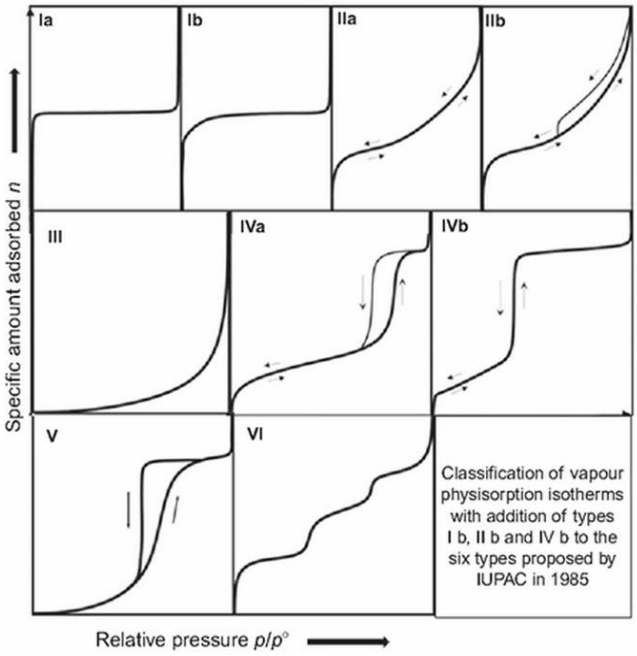

Figure 28. Classification of adsorption isotherms.[97]
(Ia): narrow micropores;
(Ib): wider micropores;
(IIa): non-porous or macroporous material;
(IIb): Aggregated particles, causing hysteresis;
(III): non-porous or macroporous material with weak adsorbate-adsorbent interactions;
(IVa): Mesoporous material, capillary condensation is causing the hysteris loop;
(IVb) ordered mesoporous material;
(V) Rare mesoporous or microporous material;
(VI): Layer-by-layer adsorption on a highly uniform surface.

The surface area, pore volume, pore area, external area and pore volume can be calculated from the isotherms with a few assumptions, which will not be discussed here but can be found in reference [97].

Instrumentation

N_2-physisorption experiments were performed on a Micrometrics TriStar 3000 V6.08 A. The isotherms were measured at -196 °C. Prior to the measurement, the samples were heated to 300 °C for 1200 minutes. The specific surface areas were estimated using the BET approach. Pore volumes were determined by fitting the isotherm to a t-plot of alumina/silica.

4.7 Atomic Absorption Spectrometry

Dissolved metal ions in aqueous solution can be measured and quantified with the use of AAS. The solution is vaporized or nebulized and subsequently heated by a flame to fully evaporate and more importantly: to atomize the elements in the sample.

As the ions are atomized, a light shines through the flame to measure the absorption of the atoms. As in other spectroscopic techniques, electrons in the atoms can be excited to higher energy levels and will absorb a photon of a specific wavelength during this process. To measure one specific element in the flame, a hollow cathode lamp is often used.

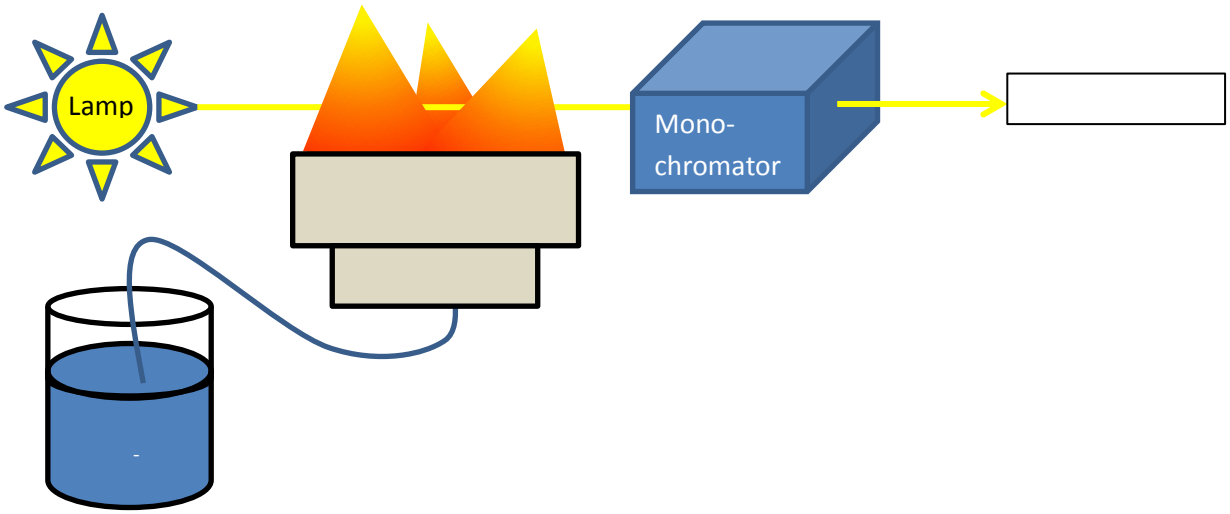

Figure 29. A simplified drawing of an AAS set-up. A solution containing the ions which are to be measured is sucked up through a tube and is subsequently nebulized before it is being atomized by a flame. The atomized material is then analyzed with a lamp that emits the same wavelength as the characteristic absorption energy of the particular element.

With increasing metal concentration, more metal atoms will be present in the flame, which in its turn cause higher absorption intensities. By preparing a set of samples with a known concentration on the same day of the measurement, a calibration line can be made. Since AAS is such a well-known method, the optimal concentration ranges for different solutions have already been published and are used in this thesis.[98]

Instrumentation

AAS measurements were performed on a ContrAA® 300 atomic absorption spectrometer supplied by Analytik Jena. The elements were atomized in an acetylene/air flame of which the ratio was optimized by the supplied software and a xenon short-arc lamp was used.

Sample preparation

10 mg of the ZIF is dissolved in 1 mL 65% nitric acid and 9 mL demineralized water. 25 µL from this solution is then diluted 400 times with DI water in a 10 mL volumetric flask.

Calibration line preparation

A 1 g/L aqueous zinc ion stock solution was made by dissolving 0.31 g ZnO in 10 mL 65% nitric acid and 240 mL DI water in a 250 mL volumetric flask. To dissolve all the ZnO particles and to obtain a homogeneous mixture, the flask was tilted 15 times. Just before making the calibration line, the stock solution was further diluted to 10 µg/mL by diluting 0.1 mL in a 10 mL volumetric flask with DI water. The solutions for the calibration line were prepared as described in Table A 7.

A 1 g/L aqueous manganese ion stock solution was made by dissolving 0.33 g MnO in 25 mL 65% nitric acid and 240 mL DI water in a 250 mL volumetric flask. The mixture was put in an ultrasonic bath for 5 minutes to dissolve all particles and to obtain a clear solution, the flask was then tilted 15 times to obtain a homogeneous solution. Just before making the calibration line, the stock solution was further diluted to 10 µg/mL by diluting 0.1 mL in a 10 mL volumetric flask with DI water. The solutions for the calibration line were prepared as described in Table A 7.

4.8 Inductively Coupled Plasma Optical Emission Spectrometry

Inductively Coupled Plasma Optical Emission Spectrometry (ICP-OES) is comparable with AAS; dissolved samples are introduced to the instrument. Just as with AAS, the solution is nebulized into an aerosol. Instead of using a flame, the aerosol is introduced to the plasma by an argon flow. The plasma gas of argon will first atomize all the ions and is also able to excite and ionize most of the elements in the periodic table. Although the real mechanism is not known for excitation and ionization of the elements in plasma, it is thought that it is caused by collisions of electrons and atoms in the plasma. When excited atoms relax to their ground state, they will emit photons with characteristic energies of which their intensities can be used for quantitative measurements.[99] This is in contrast to AAS, where the absorption of the incoming light is measured.

An important benefit of ICP over flames is that the temperatures are greatly increased in comparison to flames, 6800 K for plasmas over a maximum of 3300 for flames. This increases efficiencies as well as chemical interferences.

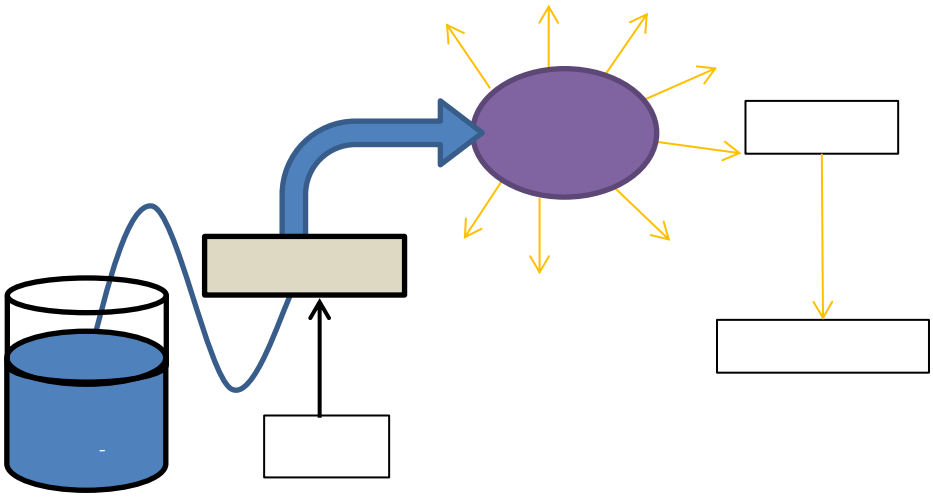

Figure 30. A simplified model of an ICP-OES set-up. A solution with the dissolved sample is sucked up into a nebulizer and is then carried with argon gas to the plasma. Because of the high temperatures in the plasma, the atoms can get excited to higher energy levels and relax thereafter by emitting light with a characteristic energy.

Instrumentation

ICP-OES measurements were performed on a SpectroBlue supplied by the firm Spectro Analytical Instruments GmbH with an End On Plasma system, using an argon plasma. The introduction system used for the samples was a Cross Flow Nebulizer with a Scott Spray Chamber and a Fixed Torch 1.8 mm.

4.9 X-ray Photoelectron Spectroscopy

X-ray Photoelectron Spectroscopy (XPS) has proven to be a very effective and popular method to analyze the surfaces of materials. Its popularity comes from the fact that with minimal sample preparation and with relative ease, the chemical composition of the outer 10 nm of a material can be identified and qualified. Almost all elements can be identified, excluding hydrogen and helium, and even their chemical environment and oxidation state can be determined.[14]

XPS works on the principle that electrons from the elements within the sample can be ejected from their orbital by a high energy photon. The photons that interact with the matter are annihilated and since they are massless, a full energy conversion takes place. If the energy of the incoming photon is high enough, electrons will be emitted from the atoms and/or ions that are present in the substrate its surface. An analyzer will then measure a fraction of the emitted electrons with a certain kinetic energy (E_k); this is not an intrinsic material property but instead is dependent on the energy of the photons. With this experiment, the binding energy (E_b) for the species in roughly the first 10 nm of the material can then be calculated if the energy of the photons (*hv*) and the work function of the spectrometer (*W*) are known:[100]

$$E_B = hv - E_k - W$$

X-rays are able to penetrate material to a few µm deep and will cause elements from within the material to emit electrons throughout this penetration depth. However, photoelectrons will not have such a large mean free path and as a result, only electrons close to the surface can escape easily without having a too large percentage colliding with other species at the surface. As a result, emitted photoelectrons deeper than 10 nm will never reach the spectrometer without losing their characteristic energies; this makes it an ideal surface analysis method.[100] Electrons that did lose energy by colliding will not have a characteristic energy, and will only result in an increase in the noise. This is causing the step-like increase in noise in XPS spectra.

XPS can be used for the qualification of samples as well as for quantification. Percentages of all elements present can be calculated relatively easy under the assumption that the material is homogeneous within the volume sampled by XPS. By calculating the peak areas of all the elements detected by XPS, it is possible to calculate atomic percentages.

Instrumentation

XPS measurements were carried out on a Thermo Fisher K-ALPHA instrument using Al Kα (1486.6 eV) radiation as an excitation source. For survey scans, a constant pass energy of 100 eV was used and for region scans a constant pass energy of 50 eV was used. The base pressure in the analysis chamber was below $8 \cdot 10^{-8}$ mbar.

4.10 Scanning Electron Microscopy and Energy Dispersive X-ray Spectroscopy

With scanning electron microscopy (SEM), high energy electrons are focused on a substrate and a scan is made of the surface. Multiple phenomena can take place when the electrons hit the surface (Figure 31). Secondary electrons are electrons with energies between 0 and 50 eV; they are emitted by the substrate when hit by the electron beam. As a result of their low energy, they will travel a short distance through the sample (3-10 nm from the surface) and will carry high resolution information of the surface because they are formed at the place where the incident beam hits the specimen.

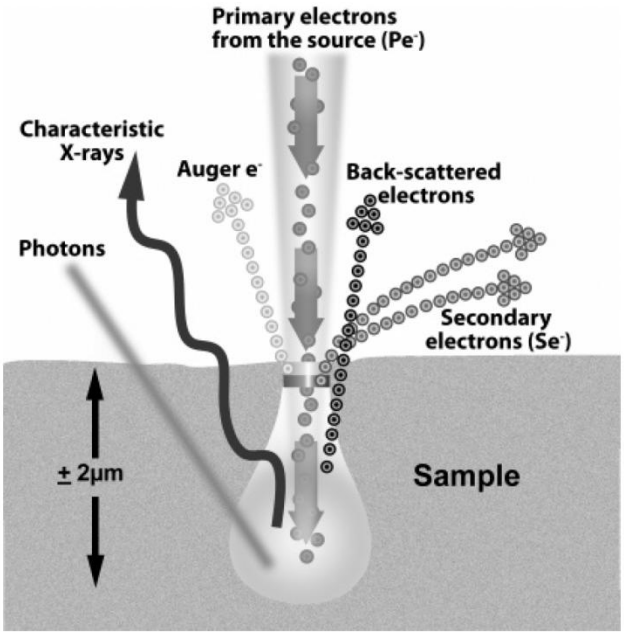

Figure 31. The incident electron beam interacts with the substrate in different ways and causes the excitation of characteristic X-rays for EDX, BSE and SE for SEM and Auger electrons.[104]

Instead of interacting with the electrons in the sample, electrons from the beam can also be scattered by the sample. These electrons possess energies of above 50 eV and are called back-scattered electrons (BSE). Detection of BSE can give additional information on the composition of the material. [101]

When matter is hit by a beam of electrons with high energies, there is also a small chance that the atoms will get ionized. Electrons in the L-shell can move into the K-shell where an electron was 'pushed' out by the incoming electron into vacuum. In this process, the electron that moved from the L-shell to the K-shell will get lowered in energy and has a chance to emit an X-ray photon with the energy that is associated with this process. As all elements have specific energies, qualitative measurements can be performed on the substrate as well as quantitative measurements with the use of the intensities of specific X-ray energies. This principle is used in Energy Dispersive X-ray Spectroscopy (EDX).[102]

Instrumentation

Scanning electron microscope: XL30SFEG, made by FEI Company, Almelo, the Netherlands.

EDX measurements: EDAX, Tilburg, the Netherlands.

4.11 Atomic Force Microscopy

AFM is a method to measure and visualize the shape of a surface in three dimensional detail down to the nanometer scale (Figure 32). By keeping the tip in contact with the surface or by oscillating the tip close to the surface and moving it laterally over the surface of the substrate while measuring the vertical displacement of the tip, a height image can be obtained. A laser is pointed on a cantilever to which the tip is attached and the light is reflected to a photodiode. Height differences or chemical differences on the surface of the substrate will cause the tip and cantilever to move or oscillate in another way. These variations are gauged by changes in the position of the laser on the photodiode.

Since the distance between the cantilever and the detector is roughly thousands of times the length of the cantilever, the optical lever (laser) will greatly magnify motions of the tip (Figure 32).[103] The properties of the material that have an effect on the movement of the laser are mechanical contact force, van der Waals forces between the tip and surface, capillary forces, chemical bonding and electrostatic forces.

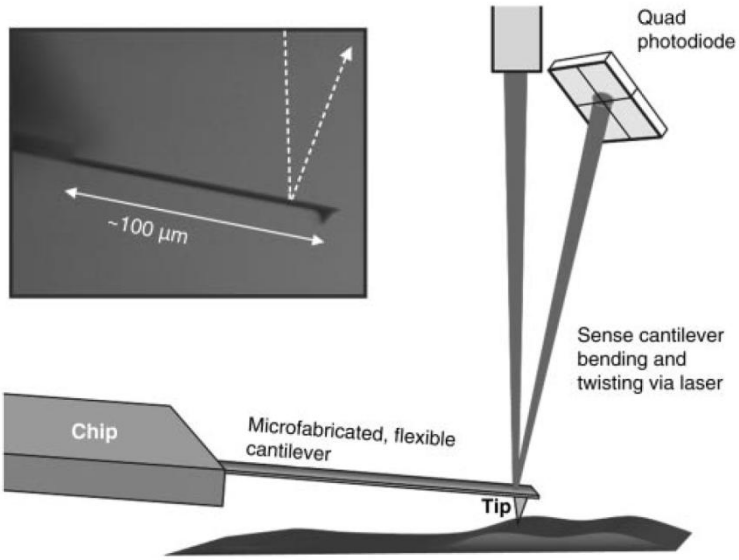

Figure 32. Schematic illustration of the basic components of an AFM instrument. A real microscopic image of a cantilever plus tip is depicted in the inset. [103]

Instrumentation

An NT-MDT NTEGRa Spectra upright AFM unit setup was used for AFM measurements. The measurements were carried out in semi-contact mode.

References

[1] H. Fei, J. F. Cahill, K. a Prather, S. M. Cohen, *Inorg. Chem.* **2013**, *52*, 4011–6.

[2] S. Bhatia, *Zeolite Catalysis: Principles and Applications*, CRC Press, Boca Raton, **2012**.

[3] A. W. Chester, E. G. Derouane, *Zeolite Characterization and Catalysis*, Springer, Dordrecht, **2009**.

[4] W. Vermeiren, J.-P. Gilson, *Top. Catal.* **2009**, *52*, 1131–1161.

[5] E. Erdem, N. Karapinar, R. Donat, *J. Colloid Interface Sci.* **2004**, *280*, 309–14.

[6] B. F. Hoskins, R. Robson, *J. Am. Chem. Soc.* **1989**, *111*, 5962–5964.

[7] H. Deng, S. Grunder, K. E. Cordova, C. Valente, H. Furukawa, M. Hmadeh, F. Gándara, A. C. Whalley, Z. Liu, S. Asahina, et al., *Science* **2012**, *336*, 1018–23.

[8] H. Deng, C. J. Doonan, H. Furukawa, R. B. Ferreira, J. Towne, C. B. Knobler, B. Wang, O. M. Yaghi, *Science* **2010**, *327*, 846–50.

[9] Z. Wang, S. M. Cohen, *J. Am. Chem. Soc.* **2009**, *131*, 16675–7.

[10] S. L. James, *Chem. Soc. Rev.* **2003**, *32*, 276.

[11] O. K. Farha, I. Eryazici, N. C. Jeong, B. G. Hauser, C. E. Wilmer, A. a Sarjeant, R. Q. Snurr, S. T. Nguyen, a Ö. Yazaydın, J. T. Hupp, *J. Am. Chem. Soc.* **2012**, *134*, 15016–21.

[12] F. J. Uribe-romo, C. B. Knobler, M. O. Keeffe, O. M. Yaghi, *Am. Chem. Soc.* **2010**, *43*, 58–67.

[13] K. S. Park, Z. Ni, A. P. Côté, J. Y. Choi, R. Huang, F. J. Uribe-Romo, H. K. Chae, M. O'Keeffe, O. M. Yaghi, *Proc. Natl. Acad. Sci. U. S. A.* **2006**, *103*, 10186–91.

[14] P. van der Heide, *X-Ray Photoelectron Spectroscopy: An Introduction to Principles and Practices*, John Wiley & Sons, Inc., **2012**.

[15] S. Nazarpour, *Thin Films and Coatings in Biology*, Springer Netherlands, Dordrecht, **2013**.

[16] L. B. Mccusker, D. H. Olson, *Atlas of Zeolite Framework Types*, Elsevier, **2007**.

[17] M. E. Davis, *Nature* **2002**, *417*, 813–821.

[18] D. Britt, D. Tranchemontagne, O. M. Yaghi, *Proc. Natl. Acad. Sci. U. S. A.* **2008**, *105*, 11623–7.

[19] D. Zacher, K. Yusenko, A. Bétard, S. Henke, M. Molon, T. Ladnorg, O. Shekhah, B. Schüpbach, T. de los Arcos, M. Krasnopolski, et al., *Chemistry* **2011**, *17*, 1448–55.

[20] S. Hermes, F. Schröder, R. Chelmowski, C. Wöll, R. a Fischer, *J. Am. Chem. Soc.* **2005**, *127*, 13744–5.

[21] Y. Li, F. Liang, H. Bux, W. Yang, J. Caro, *J. Memb. Sci.* **2010**, *354*, 48–54.

[22] A. Noy, D. V Vezenov, C. M. Lieber, in *Handb. Mol. Force Spectrosc.* (Ed.: A. Noy), MA Springer, US, Boston, **2008**, pp. 97–122.

[23] O. Shekhah, M. Eddaoudi, *Chem. Commun. (Camb).* **2013**, *49*, 10079–81.

[24] G. Lu, O. K. Farha, W. Zhang, F. Huo, J. T. Hupp, *Adv. Mater.* **2012**, *24*, 3970–4.

[25] M. C. McCarthy, V. Varela-Guerrero, G. V Barnett, H.-K. Jeong, *Langmuir* **2010**, *26*, 14636–41.

[26] C. Dimitrakakis, B. Marmiroli, H. Amenitsch, L. Malfatti, P. Innocenzi, G. Grenci, L. Vaccari, A. J. Hill, B. P. Ladewig, M. R. Hill, et al., *Chem. Commun. (Camb).* **2012**, *48*, 7483–5.

[27] C. Hou, Q. Xu, J. Peng, Z. Ji, X. Hu, *Chemphyschem* **2013**, *14*, 140–4.

[28] G. Lu, J. T. Hupp, *J. Am. Chem. Soc.* **2010**, *132*, 7832–3.

[29] S. Li, W. Shi, G. Lu, S. Li, S. C. J. Loo, F. Huo, *Adv. Mater.* **2012**, *24*, 5954–8.

[30] C. Munuera, O. Shekhah, H. Wang, C. Wöll, C. Ocal, *Phys. Chem. Chem. Phys.* **2008**, *10*, 7257–61.

[31] S. Qiu, G. Zhu, *Coord. Chem. Rev.* **2009**, *253*, 2891–2911.

[32] D. Zacher, O. Shekhah, C. Wöll, R. a Fischer, *Chem. Soc. Rev.* **2009**, *38*, 1418–29.

[33] Y. Yoo, H.-K. Jeong, *Chem. Commun. (Camb).* **2008**, 2441–3.

[34] Y.-S. Li, F.-Y. Liang, H. Bux, A. Feldhoff, W.-S. Yang, J. Caro, *Angew. Chem. Int. Ed. Engl.* **2010**, *49*, 548–51.

[35] E. Biemmi, C. Scherb, T. Bein, *J. Am. Chem. Soc.* **2007**, *129*, 8054–5.

[36] O. Shekhah, H. Wang, S. Kowarik, F. Schreiber, M. Paulus, M. Tolan, C. Sternemann, F. Evers, D. Zacher, R. a Fischer, et al., *J. Am. Chem. Soc.* **2007**, *129*, 15118–9.

[37] F. Tao, S. L. Bernasek, *Chem. Rev.* **2007**, *107*, 1408–53.

[38] Y. Pan, Y. Liu, G. Zeng, L. Zhao, Z. Lai, *Chem. Commun. (Camb).* **2011**, *47*, 2071–3.

[39] Y. Pan, D. Heryadi, F. Zhou, L. Zhao, G. Lestari, H. Su, Z. Lai, *CrystEngComm* **2011**, *13*, 6937.

[40] K. Kida, M. Okita, K. Fujita, S. Tanaka, Y. Miyake, *CrystEngComm* **2013**, *15*, 1794.

[41] A. F. Gross, E. Sherman, J. J. Vajo, *Dalton Trans.* **2012**, *41*, 5458–60.

[42] R. G. Nuzzo, D. L. Allara, *J. Am. Chem. Soc.* **1983**, *105*, 4481–4483.

[43] E. B. T. Y. Tao, J. Evall, **1989**, *335*, 321–335.

[44] H. Ron, S. Matlis, I. Rubinstein, *Langmuir* **1998**, *14*, 1116–1121.

[45] J. C. Love, L. a Estroff, J. K. Kriebel, R. G. Nuzzo, G. M. Whitesides, *Chem. Rev.* **2005**, *105*, 1103–69.

[46] D. Kisailus, Q. Truong, Y. Amemiya, J. C. Weaver, D. E. Morse, *Proc. Natl. Acad. Sci. U. S. A.* **2006**, *103*, 5652–7.

[47] G. T. Hermanson, “Bioconjugate Techniques,” **2008**.

[48] K. S. Park, Z. Ni, A. P. Côté, J. Y. Choi, R. Huang, F. J. Uribe-Romo, H. K. Chae, M. O’Keeffe, O. M. Yaghi, *Proc. Natl. Acad. Sci. U. S. A.* **2006**, *103*, 107–218.

[49] J. Qian, F. Sun, L. Qin, *Mater. Lett.* **2012**, *82*, 220–223.

[50] G. Socrates, *Infrared and Raman Characteristic Group Frequencies Contents*, John Wiley & Sons, Ltd, Chichester, UK, **2001**.

[51] C.-W. Chang, J.-D. Liao, *Nanotechnology* **2008**, *19*, 315703.

[52] S. K. Arya, P. R. Solanki, R. P. Singh, M. K. Pandey, M. Datta, B. D. Malhotra, *Talanta* **2006**, *69*, 918–26.

[53] R. Arnold, W. Azzam, A. Terfort, C. Wo, **2002**, 3980–3992.

[54] T. M. Willey, A. L. Vance, T. Van Buuren, C. Bostedt, A. J. Nelson, L. J. Terminello, C. S. Fadley, *Langmuir* **2004**, *20*, 2746–2752.

[55] J. W. Niemantsverdriet, I. Chorkendorff, in *Concepts Mod. Catal. Kinet.*, Wiley-VCH Verlag GmbH & Co. KGaA., Weinheim, Germany, **2003**, pp. 1–21.

[56] K. Kervinen, P. C. a Bruijnincx, A. M. Beale, J. G. Mesu, G. van Koten, R. J. M. Klein Gebbink, B. M. Weckhuysen, *J. Am. Chem. Soc.* **2006**, *128*, 3208–17.

[57] D. Brunel, N. Bellocq, P. Sutra, A. Cauvel, M. Laspéras, P. Moreau, F. Di Renzo, A. Galarneau, F. Fajula, *Coord. Chem. Rev.* **1998**, *178-180*, 1085–1108.

[58] A. Lu, R. K. O. Reilly, *Curr. Opin. Biotechnol.* **2013**, *24*, 638–645.

[59] J. Lee, O. K. Farha, J. Roberts, K. a Scheidt, S. T. Nguyen, J. T. Hupp, *Chem. Soc. Rev.* **2009**, *38*, 1450–9.

[60] S. J. Rettig, A. Storr, D. a Summers, R. C. Thompson, J. Trotter, *Can. J. Chem.* **1999**, *77*, 425–433.

[61] M. Kim, J. F. Cahill, H. Fei, K. a Prather, S. M. Cohen, *J. Am. Chem. Soc.* **2012**, *134*, 18082–8.

[62] M. Kim, J. F. Cahill, Y. Su, K. a. Prather, S. M. Cohen, *Chem. Sci.* **2012**, *3*, 126.

[63] O. Karagiaridi, M. B. Lalonde, W. Bury, A. a Sarjeant, O. K. Farha, J. T. Hupp, *J. Am. Chem. Soc.* **2012**, *134*, 18790–6.

[64] S. R. Venna, J. B. Jasinski, M. a Carreon, *J. Am. Chem. Soc.* **2010**, *132*, 18030–3.

[65] T. Katsuki, *Coord. Chem. Rev.* **1995**, *140*, 189–214.

[66] S. Bhattacharjee, D.-A. Yang, W.-S. Ahn, *Chem. Commun. (Camb).* **2011**, *47*, 3637–9.

[67] D. Darling, “Terrestrial Abundance of Elements,” can be found under http://www.daviddarling.info/encyclopedia/E/elterr.html, **2013**.

[68] S. Das, H. Kim, K. Kim, *J. Am. Chem. Soc.* **2009**, *131*, 3814–5.

[69] M. Kim, J. F. Cahill, H. Fei, K. a Prather, S. M. Cohen, *J. Am. Chem. Soc.* **2012**, *134*, 18082–8.

[70] X. Song, S. Jeong, D. Kim, M. S. Lah, *CrystEngComm* **2012**, *14*, 5753.

[71] L. Mi, H. Hou, Z. Song, H. Han, H. Xu, Y. Fan, S. Ng, *Cryst. Growth Des.* **2007**, *7*, 2553–2561.

[72] L. Mi, H. Hou, Z. Song, H. Han, Y. Fan, *Chem. A Eur. J.* **2008**, *14*, 1814–21.

[73] M. Lalonde, W. Bury, O. Karagiaridi, Z. Brown, J. T. Hupp, O. K. Farha, *J. Mater. Chem. A* **2013**, *1*, 5453.

[74] T. K. Prasad, D. H. Hong, M. P. Suh, *Chemistry* **2010**, *16*, 14043–50.

[75] C.-Y. Sun, C. Qin, X.-L. Wang, G.-S. Yang, K.-Z. Shao, Y.-Q. Lan, Z.-M. Su, P. Huang, C.-G. Wang, E.-B. Wang, *Dalton Trans.* **2012**, *41*, 6906–9.

[76] I. J. Kang, N. A. Khan, E. Haque, S. H. Jhung, *Chemistry* **2011**, *17*, 6437–42.

[77] K. P. de Jong, *Synthesis of Solid Catalysts*, Wiley-VCH Verlag GmbH & Co. KGaA, Weinheim, Germany, **2009**.

[78] R. H. Crabtree, *The Organometallic Chemistry of the Transition Metals*, John Wiley & Sons, Inc., Hoboken, **2009**.

[79] P. Atkins, T. Overton, J. Rourke, M. Weller, F. Armstrong, *Inorganic Chemistry*, Oxford University Press, Oxfrd, **2006**.

[80] S. Sjöberg, *Critical Evaluation of Stability Constants of Metal-Imidazole and Metal-Histamine Systems*, Umea, **1997**.

[81] W. Lian, Y. Sun, B. Wang, N. Shan, T. Shi, *J. Serbian Chem. Soc.* **2012**, *77*, 335–348.

[82] J. Dupin, D. Gonbeau, A. Levasseur, P. Cedex, T. Cedex, *Phys. Chem. Chem. Phys.* **2000**, *2*, 1319–1324.

[83] G. Beamson, D. Briggs, *High Resolution XPS of Organic Polymers, the Scienta ESCA300 Database*, Wiley, Chichester, UK, **1992**.

[84] G. T. Baronetti, O. A. Scelza, A. A. Castro, V. C. Corberan, *Appl. Catal.* **1990**, *61*, 311–328.

[85] S.-H. Cho, B. Ma, S. T. Nguyen, J. T. Hupp, T. E. Albrecht-Schmitt, *Chem. Commun. (Camb).* **2006**, 2563–5.

[86] K. S. Suslick, P. Bhyrappa, J.-H. Chou, M. E. Kosal, S. Nakagaki, D. W. Smithenry, S. R. Wilson, *Acc. Chem. Res.* **2005**, *38*, 283–91.

[87] A. F. P. Ferreira, M. C. Mittelmeijer-Hazeleger, M. A. Granato, V. F. D. Martins, A. E. Rodrigues, G. Rothenberg, *Phys. Chem. Chem. Phys.* **2013**, *15*, 8795–804.

[88] J.-R. Li, R. J. Kuppler, H.-C. Zhou, *Chem. Soc. Rev.* **2009**, *38*, 1477–504.

[89] J. Zakzeski, P. C. a Bruijnincx, A. L. Jongerius, B. M. Weckhuysen, *Chem. Rev.* **2010**, *110*, 3552–99.

[90] J. Zakzeski, A. Dębczak, P. C. a. Bruijnincx, B. M. Weckhuysen, *Appl. Catal. A Gen.* **2011**, *394*, 79–85.

[91] H. Miyachi, Y. Nagatsu, *Chem. Pharm. Bull. (Tokyo).* **2002**, *50*, 1137–40.

[92] F. Thibault-Starzyk, F. Maug, in *Charact. Solid Mater. Heterog. Catal. From Struct. to Surf. React.* (Eds.: M. Che, J.C. Védrine), Wiley-VCH Verlag GmbH & Co. KGaA, **2012**, pp. 2–47.

[93] C. Méthivier, C.-M. Pradier, in *Charact. Solid Mater. Heterog. Catal. From Struct. to Surf. React.* (Eds.: M. Che, J.C. Védrine), Wiley-VCH Verlag GmbH & Co. KGaA., **2012**, pp. 255–287.

[94] K. Nakamoto, in *Infrared Raman Spectra Inorg. Coord. Compd.*, John Wiley & Sons, Inc., **2009**, pp. 1–147.

[95] C. F. . Poole, S. K. Poole, *Chromatography Today*, Elsevier, Amsterdam, **1991**.

[96] H. Kooijman, *X-Ray Crystallography*, UU, Utrecht, **2007**.

[97] J. Rouquerol, F. Rouquerol, P. Llewellyn, G. Maurin, K. S. W. Sing, *Adsorption by Powders and Porous Solids*, Burlington Elsevier Science, **2013**.

[98] Agilent Technologies, *Flame Atomic Absorption Spectrometry*, **2012**.

[99] C. B. Boss, K. J. Fredeen, *Concepts, Instrumentation and Techniques in Inductively Coupled Plasma Optical Emission Spectrometry*, Perkin Elmer, **1997**.

[100] R. Paynter, *XPS Theory*, Varennes, Québec, **n.d.**

[101] S. Amelinckx, D. van Dyck, J. van Landuyt, G. van Tendeloo, in *Electron Microsc. Princ. Fundam.*, VCH Verlagsgescllschaft MbH, Weinheim, Germany, **1997**, pp. 305–497.

[102] Y. Leng, in *Mater. Charact. Introd. to Microsc. Spectrosc. Methods*, John Wiley & Sons, **2008**, pp. 171–195.

[103] G. Haugstad, in *At. Force Microsc. Underst. Basic Modes Adv. Appl.*, JohnWiley & Sons, Inc., New Jersey, **2012**, pp. 1–32.

[104] H. Schatten, in *Scanning Electron Microsc. Life Sci.* (Ed.: H. Schatten), Cambridge University Press, Cambridge, **2012**, pp. 1–15.

Appendix

Table A 1. Exchange yield percentages according to different characterization techniques: EDX, AAS, ICP-OES and XPS.

Sample	EDX	AAS	ICP-OES	XPS
ZIF-8 23-09		1	0	3
ZIF-8 23-09 MnX-1		9.5	8.4	13.3
ZIF-8 05-09 MnX 3.2	30.6	35.4	35.3	
ZIF-8 05-09 MnX 3.1		12.3	11.2	15.6
ZIF-8 05-08 MnX 1.1		19.18		19.9
ZIF-8 05-08 MnX 1	13.79	17.78	17.39	
ZIF-8 03-09 MnX-1		2.6	2.4	6.1

Table A 2. Content of zinc and manganese in ZIF-8 framework before and after modification with PScE measured with AAS and ICP-OES. Calculated exchange yields are supplied.

Sample	Instrument	Exchange yield (%)	Metal loading (mmol/g)	Loading Zn (mmol/g)	Loading Mn (mmol/g)
ZIF-8	AAS	1.1	3.98	3.94	0.04
	ICP-OES	0.0	4.11	4.11	0.00
ZIF-8 23-09 MnX-1	AAS	9.5	4.39	3.98	0.42
	ICP-OES	8.4	4.72	4.32	0.40
ZIF-8 23-09 MnX-2	AAS	9.6	4.63	4.19	0.45
	ICP-OES	8.8	4.47	4.08	0.39
ZIF-8 05-08 MnX-1	AAS	17.8	4.78	3.93	0.85
	ICP-OES	17.4	4.67	3.86	0.81
ZIF-8 03-09 MnX-1	AAS	2.6	4.26	4.14	0.11
	ICP-OES	2.4	4.29	4.18	0.10
ZIF-8 05-09 MnX-3.1	AAS	12.3	4.57	4.01	0.56
	ICP-OES	11.2	4.59	4.07	0.51
ZIF-8 05-09 MnX-3.2	AAS	35.4	5.14	3.32	1.82
	ICP-OES	35.3	5.12	3.31	1.81
ZIF-8 20-06 MnX-3	AAS	29.6	4.51	3.17	1.33
	ICP-OES	32.0	4.81	3.27	1.54

Table A 3. A selection of ZIF-8 crystals after an exchange period of 1 day. The metal contents were obtained with AAS measurements.

Samples	% moles Mn exchanged	Metal content (mmol/g)	Content Zn (mmol/g)	Content Mn (mmol/g)
ZIF-8 23-09	1.08	3.98	3.94	0.04
ZIF-8 03.09 MnX-1.1	2.59	4.19	4.08	0.11
ZIF-8 03-09 MnX-1.3	2.62	4.26	4.14	0.11
ZIF-8 03.09 MnX-1.2	2.65	4.32	4.20	0.11
ZIF-8 04-10 MnX - 1	3.07	4.28	4.15	0.13
ZIF-8 11-10 MnX - 2	3.20	4.33	4.19	0.14
ZIF-8 04-10 MnX - 2	3.34	4.32	4.18	0.14
ZIF-8 11-10 MnX - 1	3.38	4.34	4.20	0.15
ZIF-8 28.06 MnX -1	4.12	4.43	4.25	0.18
ZIF-8 23-09 MnX -1.1	9.47	4.39	3.98	0.42
ZIF-8 23-09 MnX -1.2	9.63	4.63	4.19	0.45
ZIF-8 22.07 MnX -1	12.21	4.93	4.33	0.60
ZIF-8 05.08 MnX -1.2	16.30	4.89	4.09	0.80
ZIF-8 05.08 MnX-1.3	16.99	4.82	4.00	0.82
ZIF-8 05-08 MnX-1	17.78	4.78	3.93	0.85
ZIF-8 05.08 MnX-1.1	19.90	4.35	3.48	0.87

Table A 4. A selection of ZIF-8 crystals after an exchange period of 3 days. The metal contents were obtained with AAS measurements

Samples	% moles Mn exchanged	Metal content (mmol/g)	Content Zn (mmol/g)	Content Mn (mmol/g)
ZIF-8 05.08 MnX-3.1	5.63	4.14	3.91	0.23
ZIF-8 05.08 MnX-3.2	7.54	4.50	4.16	0.34
ZIF-8 05.09 MnX-3.1	12.26	4.57	4.01	0.56
ZIF-8 05.08 MnX-3.3	19.17	4.67	3.77	0.89
ZIF-8 20.06 MnX-3	29.58	4.51	3.17	1.33
ZIF-8 05.09 MnX-3.2	35.40	5.14	3.32	1.82

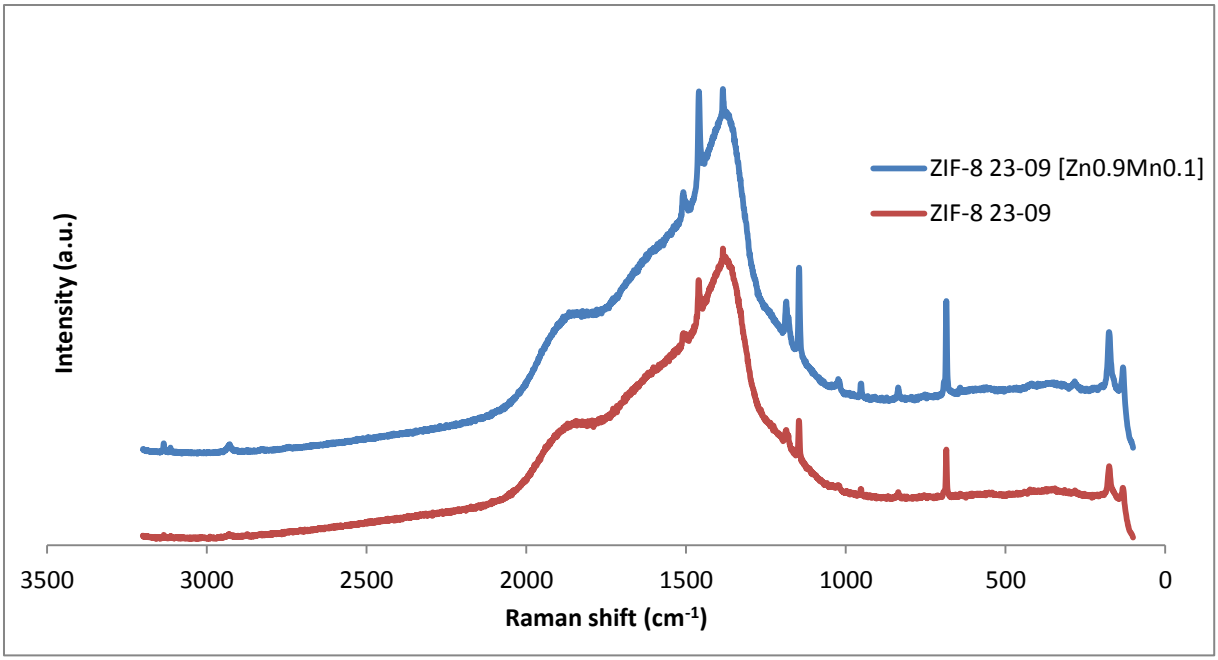

Figure A 1. Raman spectra of a ZIF-8 sample in comparison with a ZIF-8 sample with an exchange yield of 10%. No additional peaks were observed after exchanging.

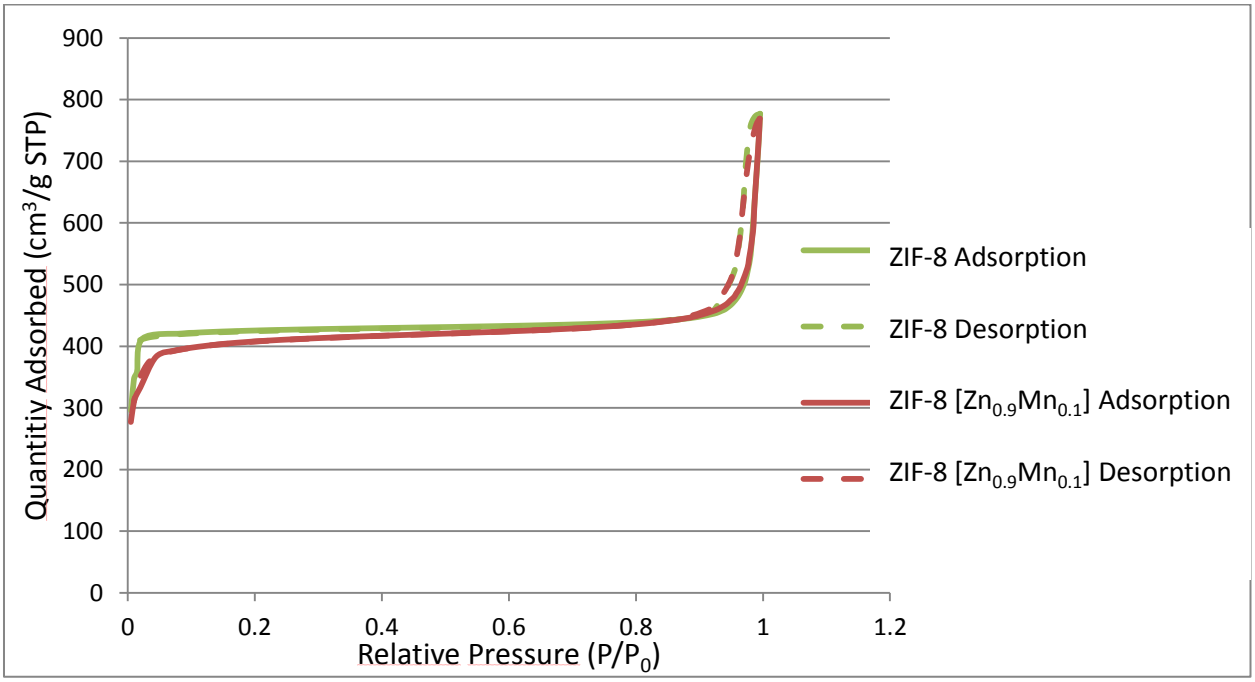

Figure A 2. N_2 physisorption isotherms of ZIF-8 compared with ZIF-8 [$Zn_{0.9}Mn_{0.1}$]. From the isotherms can be observed that the micropore volume decreases with increasing manganese content and that the isotherm also increases more between 0.1 and 0.8 P/P_0. This indicates the presence of more mesopores.

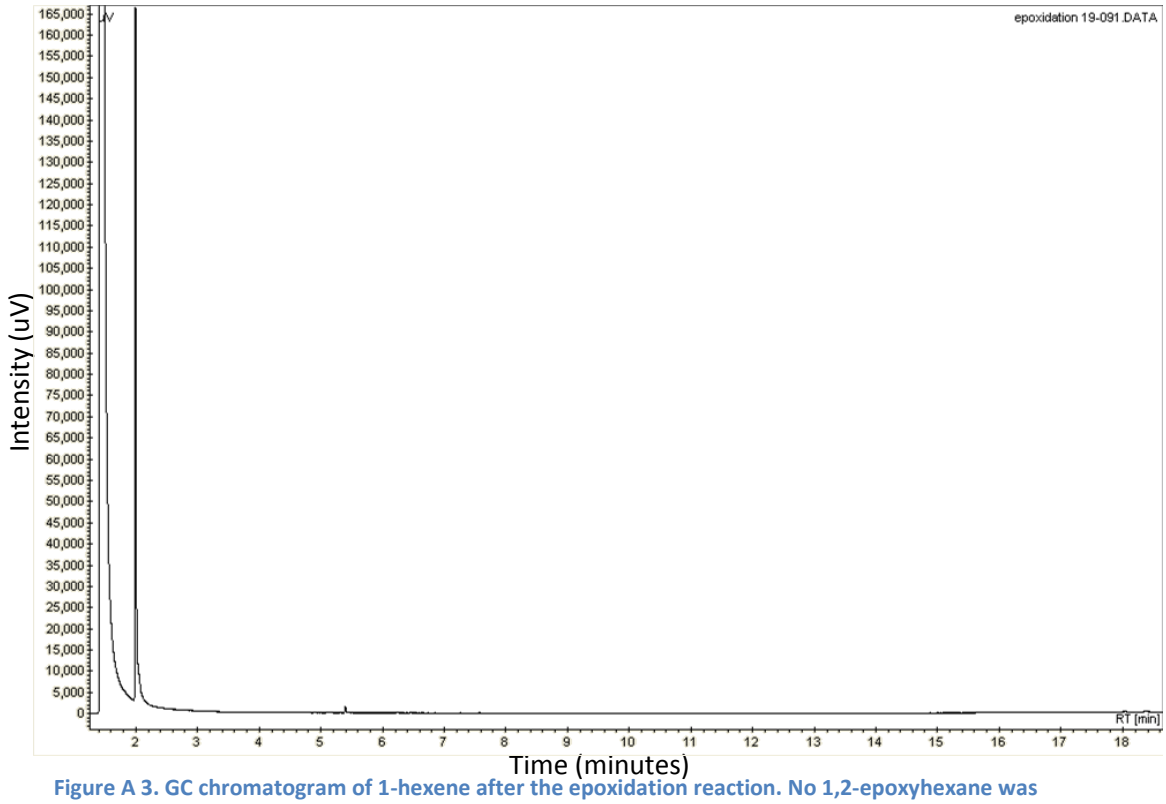

Figure A 3. GC chromatogram of 1-hexene after the epoxidation reaction. No 1,2-epoxyhexane was observed after reaction.

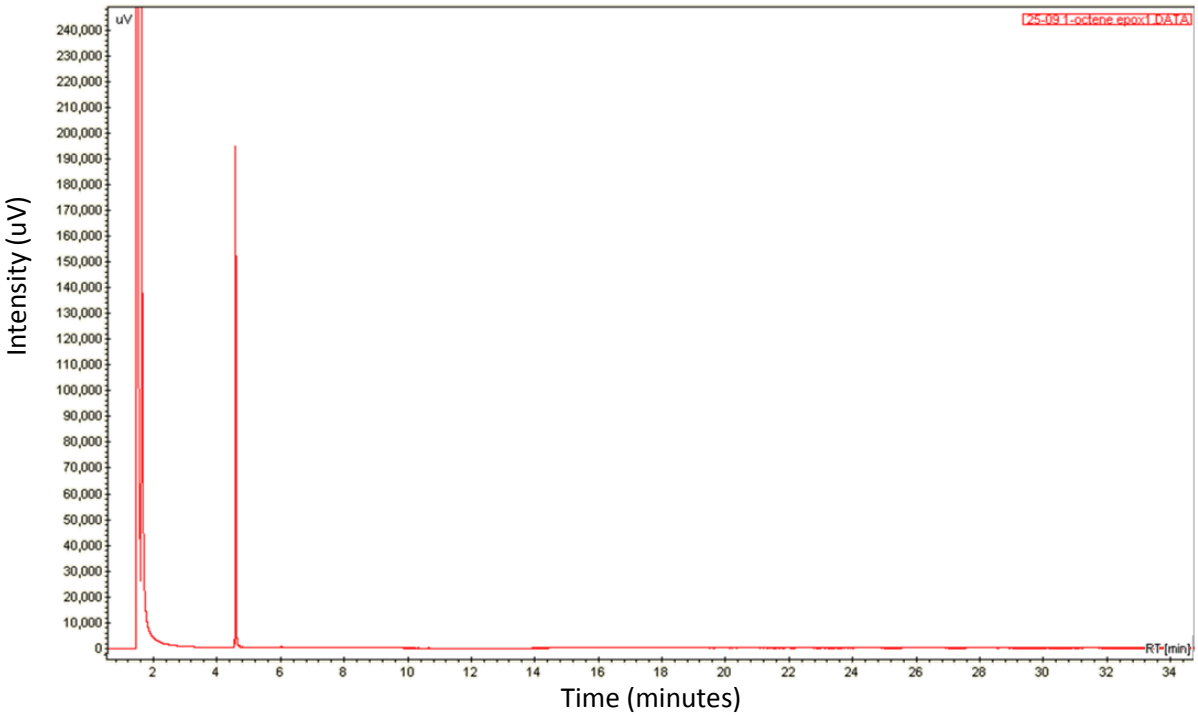

Figure A 4. GC chromatogram of 1-octene after the epoxidation reaction. No 1,2-epoxyhexane was observed after the reaction.

Table A 5. A selection of conversions of the oxidation reactions of veratryl alcohol to veratraldehyde can be found in this table.

Catalyst	conversion %
01-08 ZIF-8	9.9
05-08 ZIF-8 [$Zn_{0.7}Mn_{0.3}$]	70.9
07-08 $Mn(acac)_2$	72.4
08-08 Blank	3
01-10 ZIF-8 [$Zn_{0.81}Mn_{0.19}$]	47.6
01-10 ZIF-8 [$Zn_{0.81}Mn_{0.19}$]	47.6
02-10 Blank	20.9
11-10 Blank	24.4
15-10 ZIF-8 [$Zn_{0.81}Mn_{0.19}$]	55.3
16-10 ZIF-8	45.6
16-10 Blank	62.9

Table A 6. Assignment of the peaks in the IR spectra of Figure 23 b and c. The left part of the table describes the peaks observed for ZIF-8 [$Zn_{0.7}Mn_{0.3}$] after synthesis of the material. The right part describes the peaks observed for ZIF-8 [$Zn_{0.7}Mn_{0.3}$] after it has been used as a catalyst in the oxidation of veratryl alcohol to veratraldehyde.

ZIF-8 [$Zn_{0.7}Mn_{0.3}$] as-prepared		ZIF-8 [$Zn_{0.7}Mn_{0.3}$] post oxidation	
Band	Wavelength	Band	Wavelength
		Alcohols/water	3600-2800
Ar C-H stretch	3137	Ar C-H stretch	3137
C-H asym stretch	2975	C-H asym stretch	2975
C-H sym stretch	2934	C-H sym stretch	2934
	2162		2162
C=N stretch imidazole	1586	C=O stretch or amide	1639
			1549
CH_3 asym bend	1446-1424	CH_3 asym bend	1446
			1415
			1378
			1334
Wagging CH_2	1309	Wagging CH_2	1309
		Asym =C-O-C str	1272
		=C-H in-plane def vib	1228
			1185
	1147		1147
			1113
			1017
CH out of plane bending	998	CH in plane bending	998
NH out of plane bending	951	NH in plane bending	951

Table A 7. Preparation of solutions which were used to make a calibration line for AAS.

#	Concentration Zn^{2+} (µg/mL)	Concentration Mn^{2+} (µg/mL)	10 µg/mL Zn^{2+} solution (mL)	10 µg/mL Mn^{2+} solution (mL)	Water (mL)
1	0.2	0.02	0.2	0.02	9.78
2	0.4	0.04	0.4	0.04	9.56
3	0.6	0.06	0.6	0.06	9.34
4	0.8	0.08	0.8	0.08	9.12
5	1.0	0.12	1.0	0.12	8.88
6	1.2	0.2	1.2	0.2	8.6
7	1.4	0.4	1.4	0.4	8.2